NEW STARTING DEVICE FOR GALCIT LUDWIEG TUBE
Ae104c Project

Richard Kennedy
Jason Schlup

June 5, 2014

Advisor: Dr. Joseph Shepherd
Teaching Assistant: Bryan Schmidt

Abstract

In its current configuration, the GALCIT Ludwieg tube starts by bursting a diaphragm installed upstream of the nozzle. In this project, a new starting device was designed, built, and installed to replace the diaphragm in hopes of reducing freestream test section noise. The device is a piston-stopper system that seals in the tunnel throat and impulsively retracts to start the steady run. Numerical simulations were developed to optimize piston configuration for the design criteria. Individual parts were then designed and fabricated. After installation, full-scale tests were performed to characterize the freestream stagnation pressure fluctuations using the diaphragm and the new starting device. Preliminary data indicate that the piston start reduced the freestream noise by approximately 40 percent in the 10 - 100 kHz frequency range. Additional experimental data is needed to confirm these results.

Contents

List of Figures

List of Tables

1 Introduction and Motivation

Caltech's Ludwieg tube facility is a blowdown supersonic wind tunnel currently configured to create steady Mach 4 flow for a runtime of approximately 100 ms. In its default configuration, the tunnel uses a polycarbonate diaphragm to separate the high-pressure driver section and low-pressure driven section. When the pressure difference across the diaphragm becomes large enough the diaphragm bursts and initiates flow in the tunnel. Unfortunately, the diaphragm does not break cleanly and flutters in the tunnel during the steady test time. This feeds turbulence into the test section freestream flow. In addition, the diaphragm does not always burst at the same pressure difference, making repeating experiments difficult.

Current experiments in the GALCIT Ludwieg tube examine supersonic boundary layer transition. Disturbances in the test section flow can enter the boundary layer and provide the initial conditions necessary to grow instabilities capable of causing transition [Reshotko, 2008]. The amount of noise absorbed is known as the boundary layer's receptivity and is dependent on run conditions. Hence, it is desirable to have the test section flow devoid of as much noise as possible. (A more comprehensive examination of high speed boundary layer stability analysis can be read in Reshotko [2008].)

Ludwieg tube facilities rely on impulsively joining the driven and driver sides to create the shock-expansion wave system that propagates through the tube and starts steady supersonic flow in the test section. While the GALCIT Ludwieg tube uses a diaphragm, other facilities use a fast acting piston or valve. This reduces noise in the freestream and allows for more precise run conditions. For this study, the design conceptualization is based on a fast acting piston system employed in the hypersonic Ludwieg tube at the Technical University at Braunschweig [Estorf et al., 2004]. While the Ludwieg tube at Braunschweig operates under different conditions, a modified version of their starting technique serves as the basis of this new design. In this project, a custom fast acting piston-stopper system to replace the diaphragm in the GALCIT Ludwieg tube was conceptualized, designed, built, installed, and tested.

2 Theory and Analysis

The GALCIT Ludweig tube is a simple blowdown wind tunnel capable of producing steady supersonic flow for approximately 100 ms. It consists of four primary components: the driver side, the driven side, the nozzle, and the dump tank as shown in Figure 1. The diaphragm is placed between the driver and driven tube sections. The nozzle is a converging-diverging nozzle that produces Mach 4 flow in the test section. During operation, the gas in the driver side is pressurized until the diaphragm separating the driven and driver side bursts. At this point, a weak shock wave propagates through the nozzle and an expansion wave propagates toward the end of the driven tube. The air at the entrance of the nozzle is now highly compressed. The dump tank, which is evacuated to a low-pressure, sets a low exit pressure for the nozzle. The pressure conditions create steady supersonic flow through the nozzle and the test section. The flow remains steady until the expansion wave reaches the nozzle entrance after having returned from traveling the length of the driven tube and reflecting off the wall. At this point the pressure at the nozzle entrance is reduced such that the steady supersonic flow can no longer be maintained throughout the test section. The flow quickly becomes transient and then subsonic.

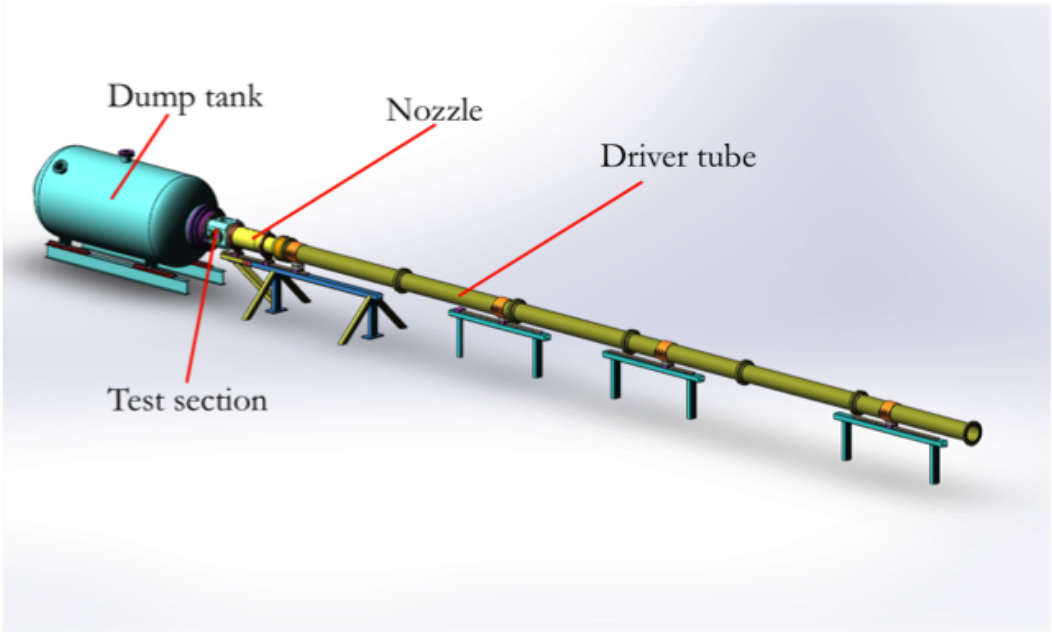

Figure 1: 3D model of the Ludwieg tube setup, including the dump tank, nozzle, test section, and driver tube.

Based on operational considerations, the fast acting piston-stopper system must meet several major criteria. The following criteria were used for the initial piston conceptualization:

a. The stopper must firmly seal at a contact diameter of 4 inches in the nozzle converging section and maintain a pressure difference between the driven and driver side

b. The piston must retract 6 inches to completely remove the stopper from the converging nozzle portion

c. The piston must fully retract in 20 ms

d. The piston must operate with a nominal driver side pressure of 5 atm.

e. The piston must remain retracted (cannot bounce back and forth)

f. The cross-sectional area of the piston housing should be minimized.

These criteria, along with cost, led to the initial design choice of using an off-the-shelf pneumatically-actuated piston. After formation of the initial concept, numerical simulations were performed to optimize the stroke length, stroke bore, and initial starting position of the piston head inside the cylinder.

3 Numerical Calculations

3.1 Nomenclature

A basic schematic describing the pneumatically actuated piston design is shown in Figure 2. In operation, the low-pressure right side is vented to atmosphere through an approximately 24 long steel tube that exits the tunnel. The stopper gets wedged in the converging section of the nozzle. To initiate a run, the left side is pressurized until the force differential on the piston head is larger than the force of the driver side gas on the stopper face. At this point the stopper unseats from the tunnel throat and the piston head impulsively accelerates towards the back of the piston.

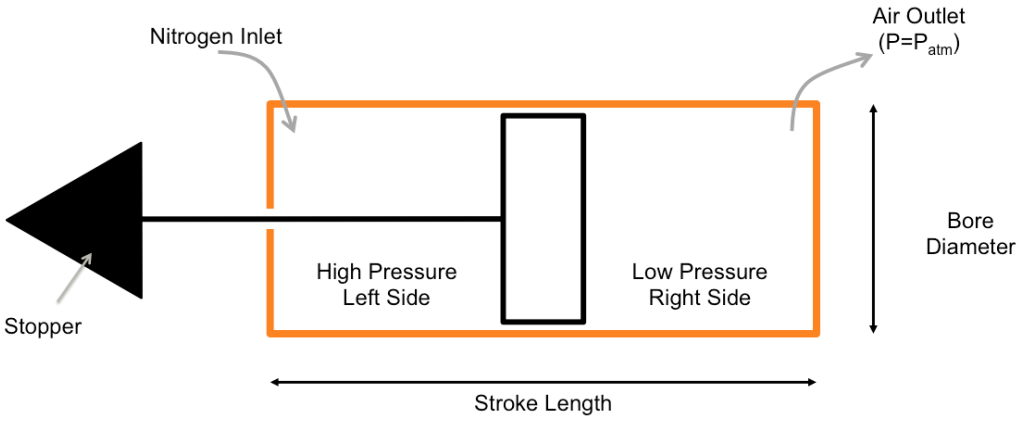

Figure 2: Conceptual cartoon of the piston-stopper system with nomenclature used in the numerical calculations.

In the numerical code described below, a subscript r or l describes either the right or left side of the piston head while a subscript i indicates an initial condition. When describing the iterative process, variables with subscript 1 represent piston vent inlet conditions while a subscript 2 represent piston vent outlet conditions.

3.2 Numerical Method

The first goal of this work was determining the necessary piston size for achieving the desired start-up time and piston travel distance. To this end, a theoretical model of the piston movement was developed using a force balance on the piston head inside the cylinder enclosure and the external pressure acting on the nozzle stopper. The following section describes the equations used to predict the piston position, velocity, and internal pressures as functions of time.

The calculations begin by specifying the fluid and piston properties. The properties used are listed in Table 1.

Table 1: Fluid and piston properties used in numerical calculations.

Air Properties		Units
Specific heat ratio (γ)	1.4	N/A
Specific gas constant (R)	640.2	$in{-}lbf/lb{-}^{\circ}R$
Temperature (T)	536.67	$^{\circ}R$
Atmospheric pressure (P_{atm})	14.7	lbf/in^2
Piston Properties		
Piston and stopper mass (m_p)	9.27	lbm
Stroke length (SL)	18	in
Bore diameter (D_{bore})	4	in
Outlet Properties		
Tube diameter (D_{out})	0.5	in
Tube length (L_{out})	20	in

After the fluid and piston properties are set, the initial starting volume on the left side and the force being applied to the stopper by the driver tube operating pressure are specified. The following method calculates the position, velocity, and pressures of the pneumatic piston.

The expansion and compression processes inside the cylinder are considered to be adiabatic and isentropic. Thus, they are governed by the isentropic process relation

$$P\left(\frac{V}{m}\right)^{\gamma} = C \tag{1}$$

where C is a constant. While the left and right sides are assumed to behave as isentropic expansions and compressions, the left side has a fixed mass while the right side loses mass as the air is forced through the vent.

The piston position is calculated by numerically solving the differential equation given as

$$F = m_p \frac{d^2x}{dt^2} \tag{2}$$

using a 4th-Order Runge-Kutta solver (ode45 in Matlab). The force in Eq. 2 is given by

$$F(t) = \left[P_l(t) - P_r(t)\right] A_P \tag{3}$$

where $P_l(t)$ and $P_r(t)$ are the time-dependent pressures on the left and right sides of the piston head, respectively, and A_P is the piston head area. $P_{l,i}$, the initial pressure on the left side of the piston head, is calculated as

$$P_{l,i} = P_{tunnel} + P_{r,i} \tag{4}$$

where $P_{r,i}$ is the initial pressure on the right piston face, set at atmospheric pressure, and P_{tunnel} is the operating pressure of the driver side; thus, $P_{l,i}$ represents the required piston pressure to unseat the stopper from the nozzle.

The two pressures in Eq. 3 are calculated from the isentropic relation given in Eq. 1. Because the initial pressure, volume, and mass on each side is known, the constant in the isentropic relation is calculated for the right and left sides.

Once C_l and C_r are known, the time-iterative process of solving Eq. 2 for $x(t)$ is done. The first step of this process is determining the stagnation pressure on the right side for the current time step from

$$\begin{aligned} P_o(t) &= C_r \left(\frac{m_r(t)}{V_r(t)} \right)^{\gamma} \\ &= C_r \left(\frac{m_r(t)}{(x_{ri} - x(t))A_P} \right)^{\gamma} \end{aligned} \tag{5}$$

After finding the stagnation pressure on the left side of the piston, a Fanno flow calculation is performed to check if the flow leaving the 20 inch long outlet tube is choked. First, using a friction factor of $f = 0.08$, the outlet tube Fanno parameter is found from

$$\frac{fL}{D} = \frac{fL_{out}}{D_{out}} \tag{6}$$

Next, upper and lower bounds on the vent inlet Mach number are found. The lower bound is assumed to be 0 (in the Matlab code, $M_1 = 1E-6$), while the upper bound is found from [Anderson, 2003]

$$\frac{fL_{out}}{D_{out}} = \left(\frac{1 - M^2}{\gamma M^2} \right) + \left(\frac{\gamma + 1}{2\gamma} \right) ln \left[\frac{M^2}{\left(\frac{2}{\gamma+1} \right) \left(1 + \frac{\gamma-1}{2} M^2 \right)} \right] \tag{7}$$

where the left side of Eq. 7 is the Fanno parameter calculated from Eq. 6. Then, the upper and lower bounds on the vent outlet Mach number, M_2, are found by first determining

the choking length, L^*, of the vent tube given the upper or lower bound of M_1. L^* is found from

$$\left(\frac{fL^*}{D_{out}}\right)_{M_1} = \left(\frac{1-M_1^2}{\gamma M_1^2}\right) + \left(\frac{\gamma+1}{2\gamma}\right) ln\left[\frac{M_1^2}{\left(\frac{2}{\gamma+1}\right)\left(1+\frac{\gamma-1}{2}M_1^2\right)}\right] \tag{8}$$

Then, the choking Fanno parameter for M_2 is calculated by

$$\left(\frac{fL^*}{D_{out}}\right)_{M_2} = \left(\frac{fL^*}{D_{out}}\right)_{M_1} - \frac{fL_{out}}{D_{out}} \tag{9}$$

and upper and lower bounds on M_2 are calculated by using the Fanno parameter from Eq. 9 in Eq. 7. If the Fanno parameter for M_2 is found to be negative, then the outlet flow is choked, and $M_2 = 1$.

Once upper and lower bounds on M_1 and M_2 have been calculated, upper and lower bounds on the static pressure at the inlet and outlet of the vent tube are determined. An isentropic flow calculation is done using the stagnation pressure inside the cylinder, P_{o1}, and the vent inlet Mach number, M_1, to find P_1 as

$$\frac{P_1}{P_{o1}} = \left(1+\frac{\gamma-1}{2}M_1^2\right)^{\frac{-\gamma}{\gamma-1}} \tag{10}$$

From Fanno flow relations, upper and lower bounds on the vent tube outlet static pressure, P_2, are calculated using

$$\frac{P_2}{P_1} = \frac{M_1}{M_2}\sqrt{\frac{1+\frac{\gamma-1}{2}M_1^2}{1+\frac{\gamma-1}{2}M_2^2}} \tag{11}$$

By using P_2 in Eq. 10, the vent outlet stagnation pressure, P_{o2}, is calculated.

An iterative process is done to determine the correct value of M_1. Beginning with the upper and lower bounds of M_1, a new guess of the vent tube inlet Mach number, $M_{1,g}$, is calculated by taking the mean of $M_{1,u}$ and $M_{1,l}$. Then, the associated outlet Mach number, $M_{2,g}$, is found using Eqs. 7 - 9 similar to finding the original upper and lower bounds of M_2. $P_{1,g}$, $P_{2,g}$, and $P_{o2,g}$ are then calculated, and $P_{o2,g}$ is compared to the known outlet stagnation pressure, $P_{o2} = P_{atm}$. If $P_{o2,g} - P_{atm} > 0$, then $M_{1,g}$ is below the actual inlet

Mach number and $M_{1,g}$ becomes the new lower bound. Otherwise, $M_{1,g}$ is too high, and $M_{1,g}$ becomes the new upper bound. Using the new bounds on M_1, a new guess of $M_{1,g}$ is made and the process is repeated until either a tolerance in $P_{o2,g} - P_{atm}$ is met (set as $1E-8$) or 100 iterations are performed. If the tolerance is not met after 100 iterations, the flow is assumed choked and M_1 is known.

Once M_1 has been determined, the stagnation density inside the cylinder is determined by using the current mass of air and volume of the right side,

$$\begin{aligned} \rho_{or}(t) &= \frac{m_r(t)}{V_r(t)} \\ &= \frac{m_r(t)}{[x_{r,i} - x_p(t)]\, A_p} \end{aligned} \tag{12}$$

Finally, the acceleration of the piston head is found using

$$\begin{aligned} a_p(t) &= \frac{[P_l(t) - P_r(t)]\, A_p}{m_p} \\ &= \frac{\left[C_l \left(\frac{m_r}{V_r(t)}\right)^{\gamma} - C_r \left(\frac{m_r(t)}{V_r(t)}\right)^{\gamma}\right] A_p}{m_p} \\ &= \frac{\left[C_l \left(\frac{m_l}{x_{l,i}+x_p(t)}\right)^{\gamma} - C_r \left(\frac{m_r(t)}{x_{r,i}-x_p(t)}\right)^{\gamma}\right] A_p^{(1-\gamma)}}{m_p} \end{aligned} \tag{13}$$

Using the current position of the piston head, the mass flow rate of air through the vent tube is calculated as

$$\begin{aligned} \dot{m} &= -\rho_1 u_1 A_{out} \\ &= -\rho_1 \sqrt{\gamma R T_1} M_1 A_{out} \\ &= -\sqrt{\gamma P_1 \rho_1} M_1 A_{out} \end{aligned} \tag{14}$$

where the air is considered an ideal gas. P_1 and ρ_1 are calculated from their stagnation properties and isentropic flow relations given in Eq. 10 for P_1 and

$$\frac{\rho_1}{\rho_{o1}} = \left[1 + \frac{(\gamma - 1)}{2} M_1^2\right]^{\frac{-1}{\gamma - 1}} \tag{15}$$

for ρ_1. In Matlab, the function call to ode45 passes a vector $\mathbf{x}$ with elements

$$\begin{pmatrix} x_1 \\ x_2 \\ x_3 \end{pmatrix} = \begin{pmatrix} x_p(t) \\ v_p(t) \\ m_r(t) \end{pmatrix} \tag{16}$$

Then, the time derivatives are given by

$$\begin{aligned} \begin{pmatrix} \dot{x}_1 \\ \dot{x}_2 \\ \dot{x}_3 \end{pmatrix} &= \begin{pmatrix} v_p(t) \\ a_p(t) \\ \dot{m}_r(t) \end{pmatrix} \\ &= \begin{pmatrix} x_2 \\ Eq.13 \\ Eq.14 \end{pmatrix} \end{aligned} \tag{17}$$

From these calculations, the piston position and velocity are exported to the main Matlab file. Using these variables, the acceleration and pressures can be calculated using the appropriate equations given above at each time step.

Many initial conditions and piston properties were tested to determine an appropriate piston size. It was found that a piston with $D_{bore} = 4$ inches and $SL = 18$ inches would meet the performance requirements. Figure 3 shows plots of the piston position, velocity, and pressure as functions of time for the selected piston size. It is important to note these calculations were done in tandem with the design of the stopper, as the material and size influences m_p in the above calculations. After the stopper design was complete, the calculations were run using the mass in Table 1 and the following results were acquired.

Figure 3a shows that in 20 ms, the piston will retract nearly 6 inches. Figure 3c indicates that at this time, the pressures on the right and left side of the piston head will be approximately equal. After 20 ms, if the piston were to stay at 6 inches, the right side pressure will begin to drop as a pressure difference from the piston to atmosphere exists. The left side pressure will remain at approximately 40 psi. Since the right side pressure will drop, the piston will not rebound towards the nozzle as the pressure on the left side will apply a force to the right on the piston head.

From Figure 3b, the piston will be traveling at nearly 450 in/s (approximately 25 mph). From these numerical results, it was possible to design the piston fairing and supports.

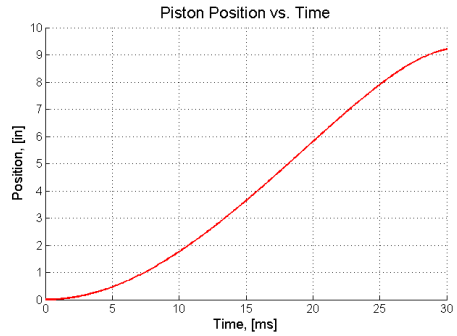

(a)

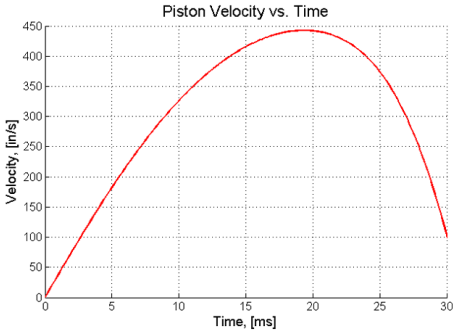

(b)

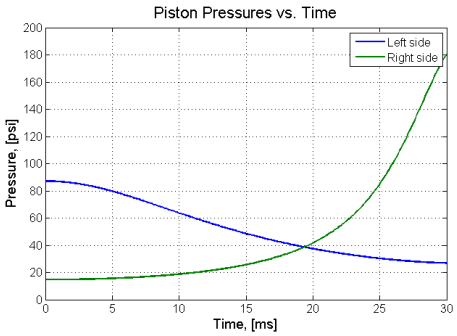

(c)

Figure 3: Results from the numerical calculations showing a) position, b) velocity, and c) pressures in the piston.

4 Design of Experimental Setup

After the numerical calculations were performed, the piston housing and supports were designed. Once the parts were finalized and machined, the equipment was tested to validate the numerical calculations prior to installing and testing the device in the Ludwieg tube.

4.1 Design of Piston-Stopper System

4.1.1 Piston

The piston was chosen to have a bore diameter of 4 inches and stroke length of 18 inches. The piston, a Parker 4.00TD4MAU19A18.00, is an off-the-shelf part to reduce costs. This piston has an aluminum head and steel shaft with female threading to attach the stopper. The piston end caps have extended tie rods which secure the piston to the front and rear housing end caps described in Sections 4.1.4 and 4.1.5. The inlet and outlet ports are NPTF threaded which allows Swagelok tube fittings and steel tubing to fill and vent the piston. Figure 4 shows a 3D model of the piston.

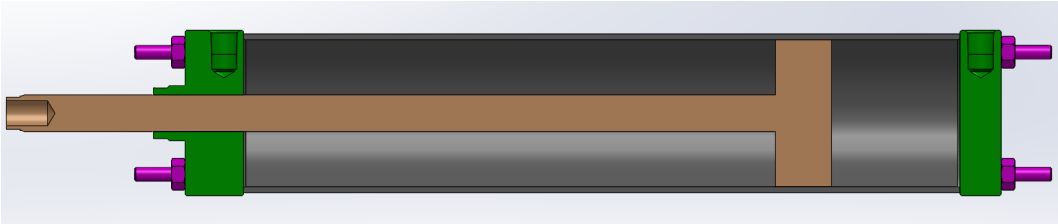

Figure 4: 3D section view of the piston, provided by Parker Pneumatic [Pneumatic, 2014]. The piston body is gray, piston head and shaft are tan, end caps are green, and tie rods are pink.

4.1.2 Stopper

The only initial requirement on the stopper was that it sealed at a 4 inch diameter in the converging section of the nozzle. While a similar device [Estorf et al., 2004] uses an entirely aluminum stopper, it was determined using a polyurethane sealing surface would ensure an adequate seal and prevent damage to the nozzle and stopper. An aluminum body was chosen over steel to reduce weight. A male-threaded rod extending past the polyurethane connects the stopper to the female threads on the piston. Figure 5 shows a 3D model of the finalized stopper design.

The aluminum diameter, left of the polyurethane in Figure 5, was chosen to be smaller than the nozzle throat in case the stopper broke during testing. Additionally, a sufficient amount of polyurethane is used so that the stopper seals the desired 4 inch diameter opening

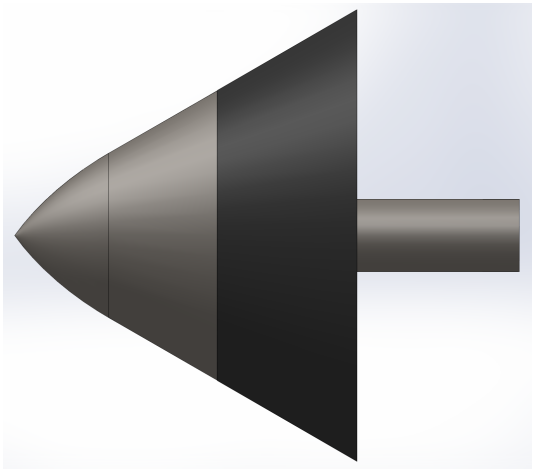

Figure 5: 3D model of the nozzle stopper. The polyurethane is colored black and the aluminum is gray in this image.

and will not slip through the nozzle once the driver side is pressurized. From the right side of Figure 5, the stopper profile is initially a straight line. The profile slowly curves towards the stopper tip with an elliptical shape.

4.1.3 Front Bumper

Once the stopper retracts from the nozzle, it remains seated against the front bumper for the remainder of the Ludwieg tube run. Thus, the profile of the front bumper and stopper were designed to prevent flow separation.

The front bumper and stopper profiles are continuous and tangent when the piston is retracted. As seen in Figure 6, the bumper has a flat profile where it attaches to the front end cap. Past this point the elliptical profile was chosen to have the required tangency with the stopper in the retracted configuration.

The inner profile is a simple hemisphere to reduce the total weight. A large hole allows the piston shaft to pass through. An additional cutout allows the polyurethane backing washer enough space to not contact the front bumper.

4.1.4 Front End Cap

The front end cap is also made from aluminum. The end cap has a central hole for the piston shaft, four threaded holes for the tie supports, and four through holes for the extended tie rods on the piston. Additionally, four slots are machined into the outer cylindrical surface where the tie supports are installed. The left side of Figure 7b has external threading that

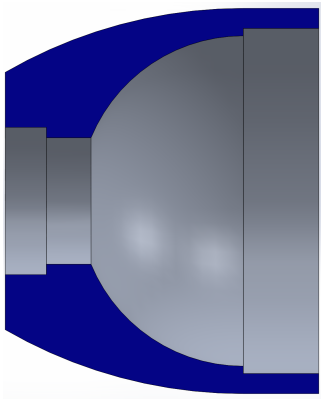

Figure 6: 3D section view of the front bumper showing the outer and inner profiles. The blue section is the cut plane.

attaches to the front bumper.

One of the challenges in designing the piston support was keeping the piston centered and level in the Ludwieg tube. This is accomplished by the four through holes in the front and rear end caps. A cylindrical external housing, made from acrylic, is needed to keep the shape streamlined. The mate between the acrylic housing and front end cap is made by the lip seal at the right end of Figure 7b, and the acrylic housing is wedged in place by securing the tie rods into the front and rear end caps. The acrylic tube and both end caps are visible in Figure 8, showing how the acrylic sits over the lip on each end cap.

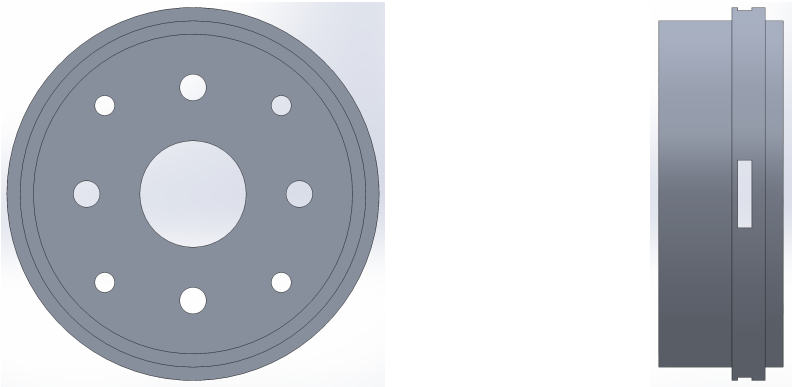

(a) (b)

Figure 7: a) Front and b) side views of the front end cap.

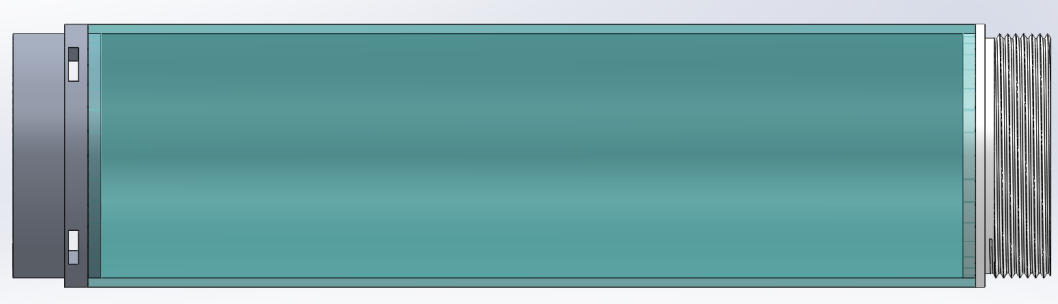

Figure 8: The acrylic housing, in transparent blue, shown around the lips of each end cap.

4.1.5 Rear End Cap and Fairing

The rear end cap is very similar to the front end cap; however, the rear end cap is made from a rapid prototyped Nylon material to reduce weight as the rear portion of the piston is cantilevered. The male threads on the rear end cap and female threads on the rear fairing were custom designed for the printing process.

The rear end cap has four through holes for the tie rod connections. Additionally, six through holes help relieve any pressure remaining in the end cap and rear fairing after the tunnel fires. Figure 9 shows a front and side view of the end cap.

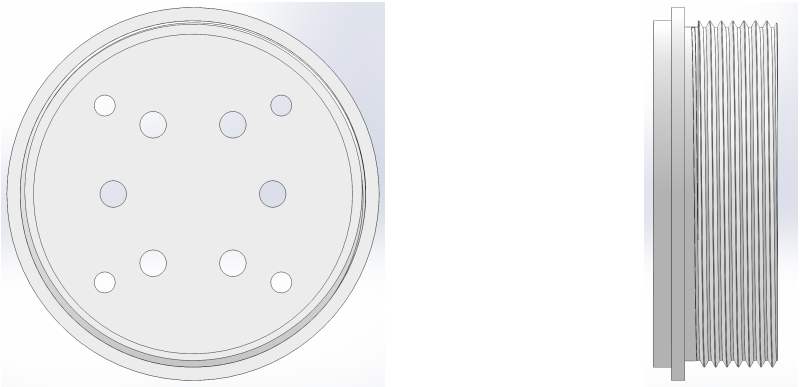

(a) (b)

Figure 9: a) Front and b) side views of the rear end cap.

The rear fairing is also rapid prototyped Nylon. The external profile is elliptical, while the internal profile removes a significant amount of mass to reduce the cantilevered force. Because the rear fairing is not load bearing, the wall can be made as thin as desired, so long as enough thickness remains for the female threading. Figure 10 shows a section view of the rear fairing. Unlike the other end caps and the front bumper, there are no holes in the surface of this part.

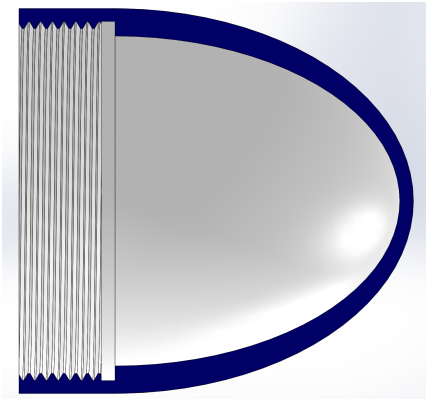

Figure 10: 3D section view of the rear fairing showing the outer and inner profiles as well as the female threading. The blue section is the cut plane.

4.1.6 Tie Supports

The final design consists of four identical tie supports, as shown in Figure 11. Each tie support is made from steel with a number of through holes. Two through holes allow connections to the nozzle-tube flange, discussed in Section 4.1.7, while one through hole allows a connection to the front end cap. The tie supports are secured into the nozzle-tube flange and front end cap with 1/2 inch Grade 8 cap screws. These connections are shown in Appendix C.

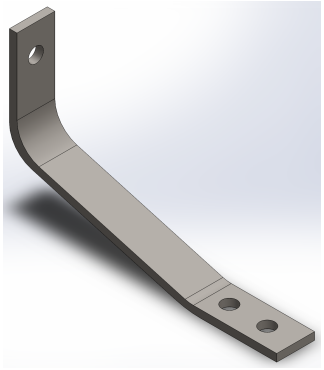

Figure 11: 3D view of the tie supports.

4.1.7 Injector Flange

The tie supports shown in Figure 11 attach to the injector flange with four cutouts. The flange is the same flange used in the diaphragm tests; for this work, new slots were machined into the inner surface. During the design, it was critical that the O-ring groove on the nozzle side of the injector flange remain untouched so that diaphragms can still be used.

Figure 12 shows the inner cylindrical surface of the flange. The hole at the top of this figure houses the injector block which contains instrumentation for the tunnel, gas fill lines for the tunnel and piston, and the piston vent. The four tie support cutouts are offset at 90° and evenly split around the injector block so the plumbing is not blocked. Figures showing the connection of the tie supports and the nozzle flange are provided in Appendix B.

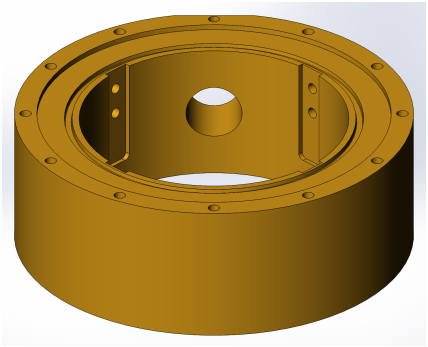

Figure 12: 3D view of the nozzle flange. The tie supports attach in the four cutouts, while the top hole runs plumbing and instrumentation.

4.2 Bench Testing

After all parts necessary to test the piston were fabricated, the system was assembled in the flange and mounted on an optical table as shown in Figure 13. Figure 13b also shows the laser range finder in the background.

In order to properly bench test the piston-stopper system, a force that could be impulsively removed needed to be applied to the stopper. The impulsive force removal simulates the stopper being unseated from the nozzle. After several experimental iterations, a method using rope was developed. One end of the rope was tied to a bar secured at the end of the optical table, and the other end was secured between the polyurethane and aluminum portions of the stopper. The cylinder was pressurized to the desired operating run pressure of the tunnel, and the rope was then cut. This sent the stopper backwards until it contacted the front bumper. The motion of the stopper was measured using a precision laser range finder (Keyence model LK-G407). A small shim was wedged between the polyurethane and aluminum portions of the stopper head to provide the range finder a flat surface for position measurements. The range finder triggered once the stopper began moving after the rope had been severed. The trigger time was set to include the motion just before the rope was severed to just after the stopper motion ceased.

Using this setup, tests simulating a tunnel pressure of approximately 220 kPa were performed. This corresponds to approximately 40% of the nominal tunnel test pressure. Higher-pressure bench tests could not be performed due to the stability of the experimental setup on the table, as well as the ultimate tensile strength of the rope.

The numerical simulation used to optimize the piston design was then modified to predict

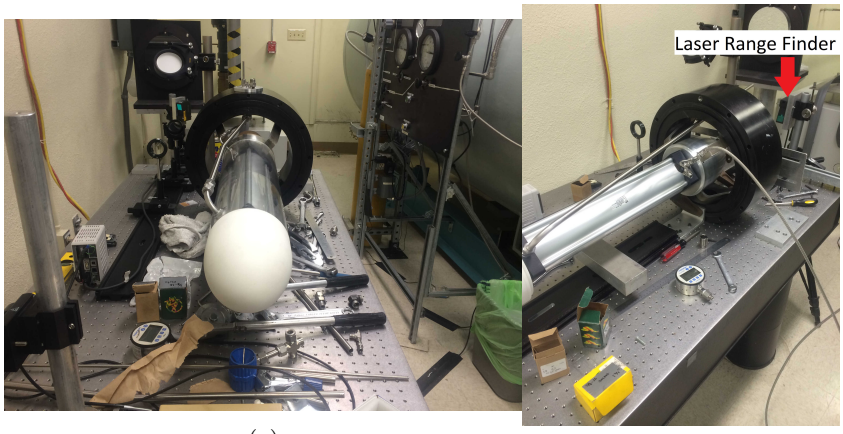

(a) (b)

(c)

Figure 13: Photographs of the bench test setup, looking at the a) rear, b) side, and c) front of the piston setup.

the motion of the piston under the bench testing conditions. The pressure in the high-pressure side of the piston was directly entered into the Matlab code. Figure 14 shows the numerical and experimental data plotted on the same graph. The slopes of the two data curves match well indicating an accurate prediction of speed after the force is removed. The time offset of the numerical simulation data and the experimental data is most likely because cutting the rope is not truly an impulsive removal of force (i.e. some fibers take longer to be cut than others). It should also be noted that the experimental data shows a steep drop at approximately 34 ms. This corresponds to the time when the stopper contacts the front bumper. This steep drop is thought to be an artifact of the shim moving just out of the range of the laser when the piston is in the fully retracted position. When this occurs the range finder returns a steady measurement value of -112.4 mm.

Another conclusion of the bench testing is the effect of elastic recoil on the piston motion. Figure 15 shows frame-by-frame images of the stopper once the rope has been cut. The

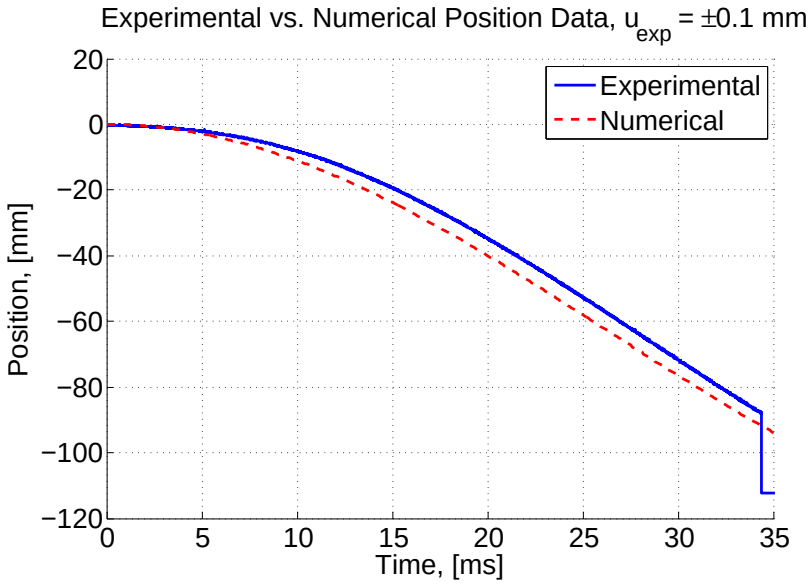

Figure 14: Comparison of numerical simulation calculations and the bench test position measurements made with the laser range finder.

stopper initially strikes the front bumper in Figure 15c. Slight recoil can be seen in Figure 15d before the stopper moves back and stays in contact with the front bumper in Figure 15e. While this recoil occurred during the bench testing, it is inconclusive whether this recoil will occur in actual run conditions as the flange experienced vibrations on the optical table that will not occur in the tunnel.

Even though slight discrepancies exist between the numerical and experimental data, the analysis indicated the piston motion is fairly well predicted by the numerical model. Based on this, the device was installed and tested in the tunnel at full-scale operating pressures.

4.3 Experimental Procedure

For each Ludwieg tube test, pressure measurements were recorded at 2 MHz using Kulite ETM-375-250A and PCB model 113A21 pressure transducers. Vezin et al. [2011] give a detailed description of the pressure transducers. They note that the PCB transducer has a discharge time of 1 second which is much longer than the testing time for this facility. They also conclude that the PCB signal, after comparison to the Kulite transducer, does not drift. The PCB transducer has a natural frequency of 500 kHz, while the Kulite sensor has a natural frequency of $\geq$ 400 kHz. With these natural frequencies, power spectral analysis can be done up to frequencies of 200 kHz, below the Nyquist frequency of the PCB sensor. The Kulite sensor measures the steady-state pressure prior to the shot, and gives the stagnation pressure during the tests. The PCB sensor is sensitive to fluctuations in the signal and measures a rapid change in stagnation pressure; thus, the PCB sensor outputs zero voltage

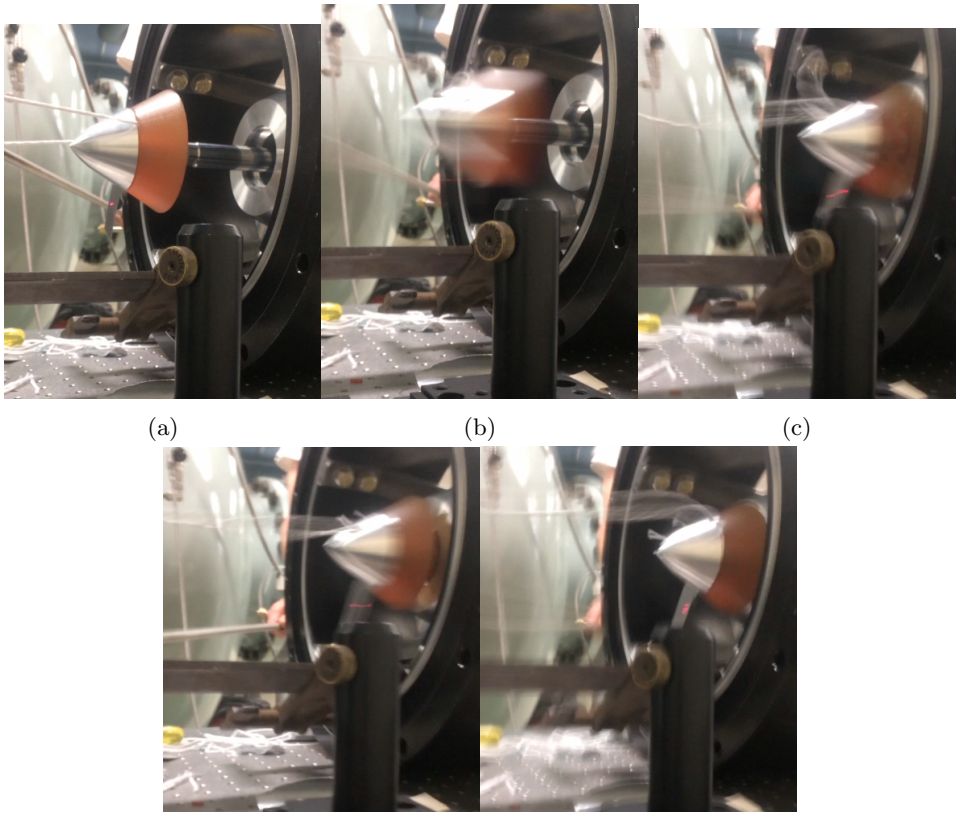

(a) (b) (c)

(d) (e)

Figure 15: Sequential screen shots of the bench test video.

at steady-state and only responds once a rapid pressure change occurs. For these tests, the Kulite sensor is used to determine the stagnation pressure, and all spectral analysis on the pressure fluctuations is performed using the PCB sensor.

For the diaphragm shots, the tunnel is opened and a new diaphragm is installed. Then, after closing the tunnel, the driver and driven sides are vacuumed down to approximately 1.5 Torr. The measurement system is armed and the driver side is filled with nitrogen until the diaphragm bursts. A burst pressure of 130 kPa(g) is typical for the 5 mil thick diaphragms.

For the piston shots, the tunnel is only opened for installation or maintenance. Once the tunnel is closed, compressed air is put into the vent side of the piston to push the stopper into the nozzle. If the tunnel is opened between shots, both the driver and driven sides are vacuumed prior to pressurizing the driver side. If the tunnel is not opened between shots, complete evacuation is not necessary and only the driven side is vacuumed to 1.5 Torr. Then, the measurement system is armed and the driver side is filled to the desired test pressure. The high-pressure side of the piston is pressurized with nitrogen until the stopper is retracted from the nozzle and the shot fires.

5 Results

Prior to installing the piston into the Ludwieg tube, three diaphragm shots were performed to acquire pressure fluctuation data. In each of these tests, the shot pressure is not controllable as the diaphragm burst pressure varies for each test.

In each spectral analysis, Welch's method with a Hann window was used. A window size of 2500 samples was selected with 50% overlap of each window.

5.1 Diaphragm Start

Three diaphragm shots were performed. Each shot has approximately the same features, including a 10 ms start time and approximately 90 ms run time. Figure 16 shows an example recording of raw voltages for a diaphragm shot, including the startup and steady run data. On occasion, a sensor records a spike in pressure; this is evidence of a piece of diaphragm hitting the transducer and is visible in high-speed video recordings from previous experiments. In this section, results from shot 269 are presented; these results are representative of each diaphragm shot. Complete results for each shot are given in Appendix A.

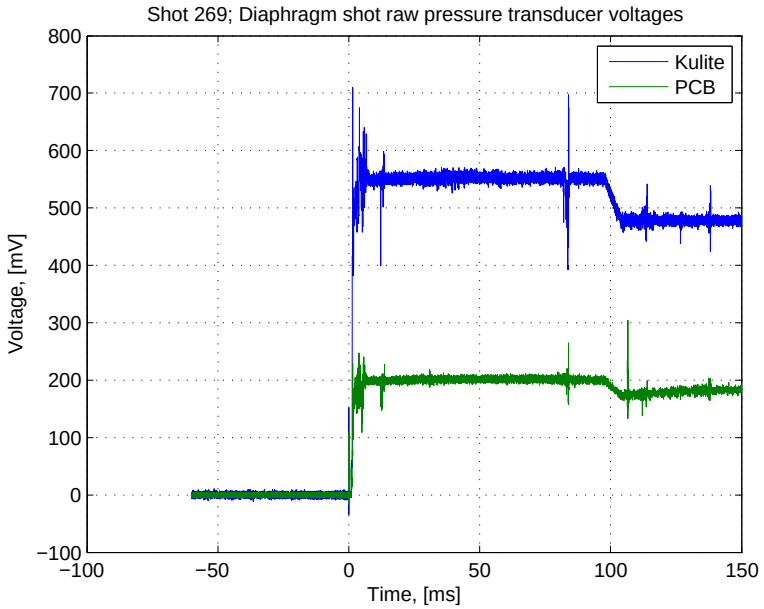

Figure 16: Raw voltages for the diaphragm shot, showing start-up and a 90 ms steady supersonic flow.

Figure 17 shows the steady run time pressures for shot 269. From this figure, it is clear that noise is present in the stagnation pressure measurements. Figure 18 shows the noise floor power spectral density (PSD) of the PCB sensor, taken at ambient conditions. The

noise floor measurement is included on the individual PSD figures for each shot to determine if the noise observed in the pressure fluctuations is caused by the instrumentation.

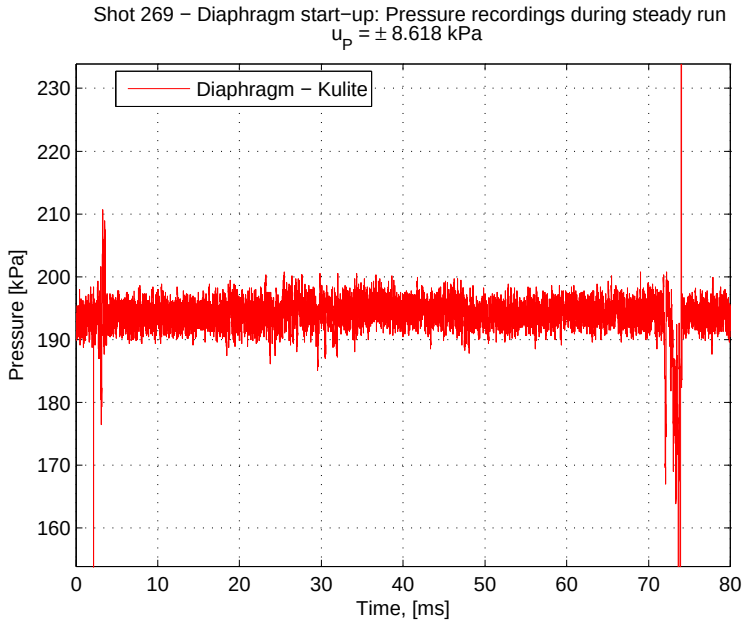

Figure 17: Steady run pressures from shot 269 using the diaphragm starting method. Large peaks in this plot are caused from diaphragm parts hitting the pressure transducers.

A power spectral density was calculated using the PCB signal and the settings given in the top of this section. Figure 19 shows the resulting PSD for the diaphragm test.

At frequencies below 100 kHz, the noise floor has a PSD orders of magnitude lower than the recorded pressure during a shot. However, above 100 kHz, the noise floor is approximately the same power as the recorded pressure fluctuations. The frequencies of interest are in the 10 - 100 kHz range so the pressure fluctuation measurements in this frequency range have enough power that the noise floor is negligible. Above 100 kHz, the digitization of the pressure fluctuations would need to be adjusted to record significant frequency content from the pressure transducers.

5.2 Piston Start

Multiple piston start datasets were taken; however, the data acquisition triggering system triggered too late to capture the steady supersonic flow for many of the shots. For the test shown below, 800 ms of data were recorded. Figure 20 shows the raw data for this piston shot.

Figure 20 indicates that the flow start-up time was approximately 50 ms and the steady supersonic flow lasted for 50 ms, shown in the figure from -200 ms to -150 ms. The longer

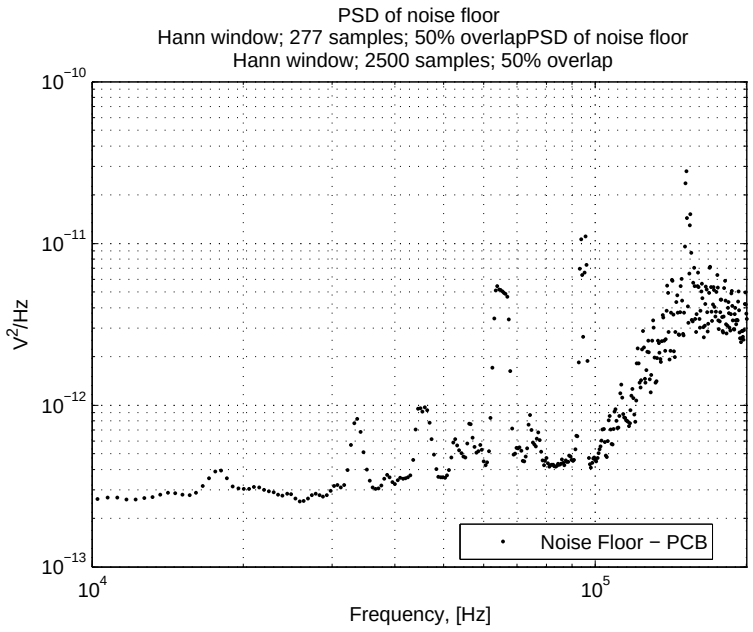

Figure 18: Noise floor PSD using the PCB transducer at ambient conditions.

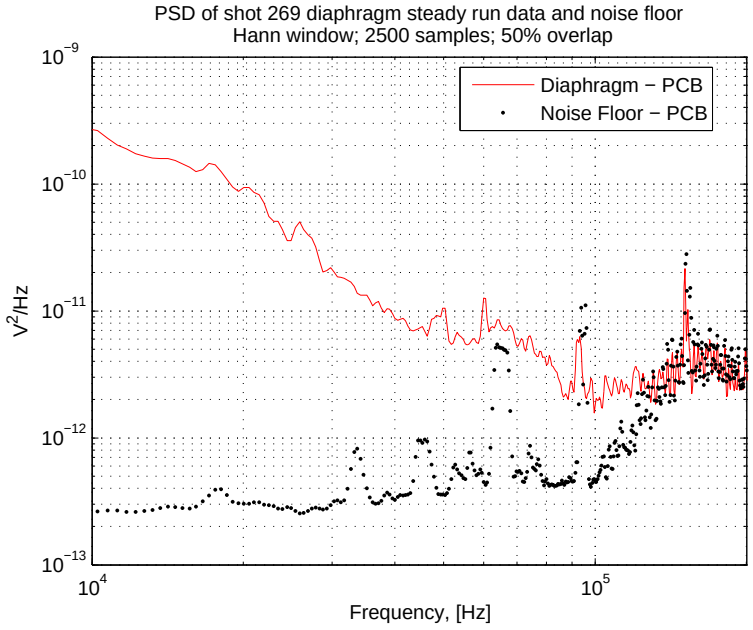

Figure 19: Diaphragm shot PSD using the PCB, including noise floor measurements.

startup time is most likely a result of the piston retracting slightly slower than predicted. This will be addressed in future work by reconfiguring the piston plumbing. The slow startup

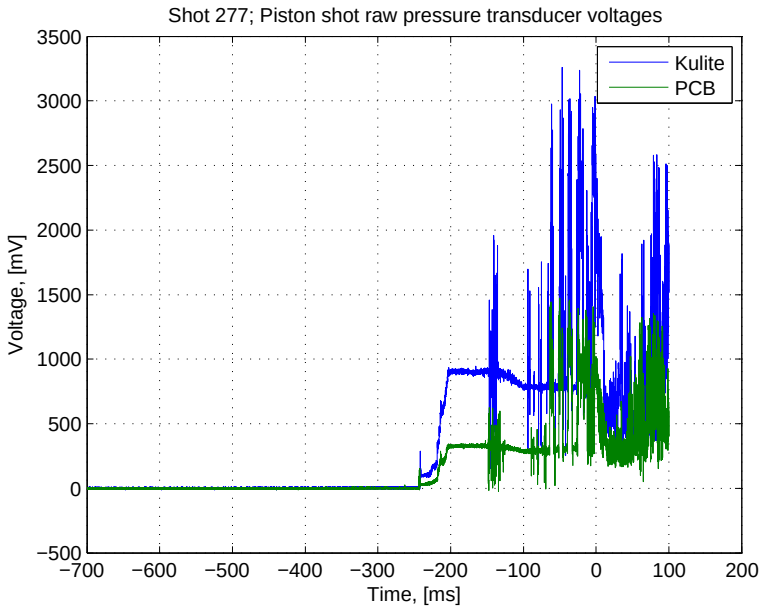

Figure 20: Raw voltages for the piston shot, showing start-up, steady supersonic flow, and unstart.

may also be an indication that the startup shock structure passing through the nozzle needed to start the flow is different that the structure produced by the bursting diaphragm. This transient startup process can be examined using high speed schlieren imaging.

Figure 21 shows the Kulite stagnation pressure recordings for the piston shot. This piston shot occurred at a higher stagnation pressure than the diaphragm shot, which is corrected when the two power spectra are compared in Section 5.3.

The steady run time pressure fluctuations are analyzed using the PCB sensor, and the resulting PSD is shown in Figure 22. Similar to the diaphragm start, the noise floor is an order of magnitude or more below the PCB signal over the frequency range of interest. Again, similar to the diaphragm shot, the noise floor at frequencies above 100 kHz is on the same order of magnitude as the pressure fluctuation data. Thus, no conclusions of the noise levels can be reliably drawn above 100 kHz.

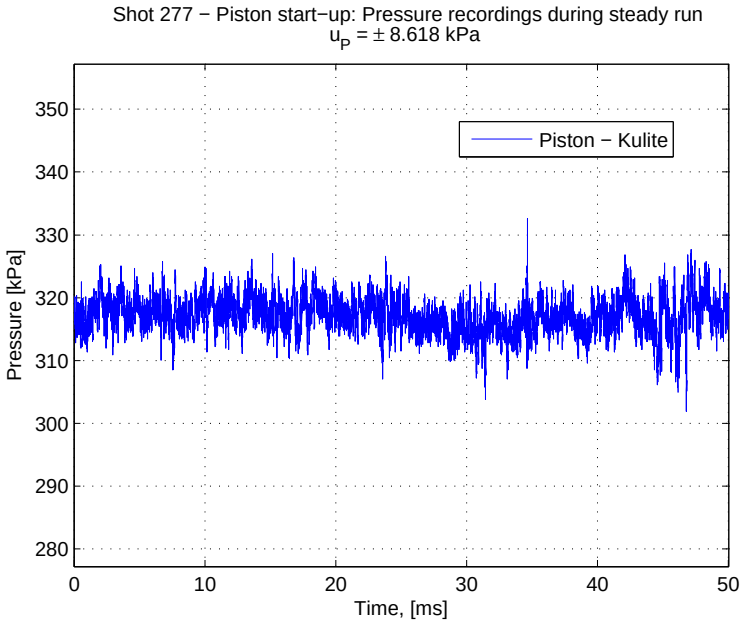

Figure 21: Steady run pressures from shot 277 using the piston to start the flow.

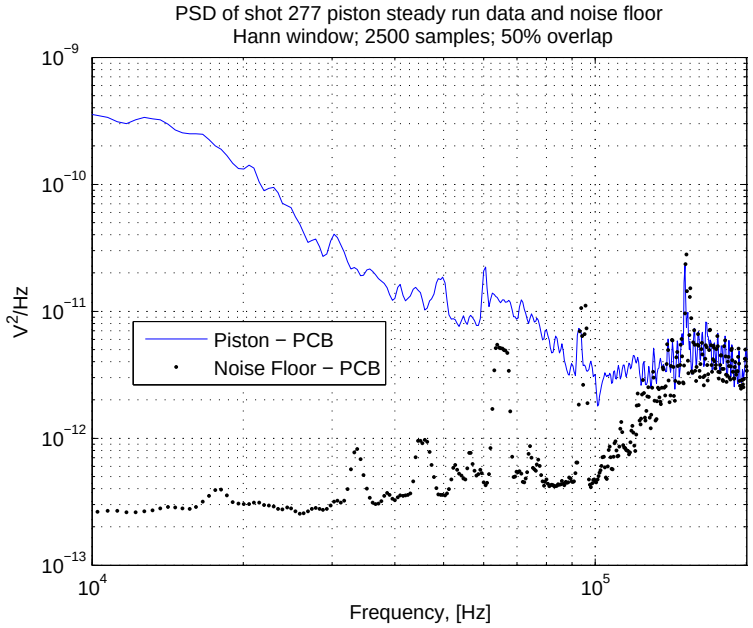

Figure 22: Piston shot PSD using the PCB, including noise floor measurements.

5.3 Noise Comparison

Once the diaphragm and piston tests were complete, a comparison of the noise levels between the two starting methods was performed. Only results from diaphragm shot 269 and piston shot 277 are presented in this section; complete results are available in Appendix A. Since the piston shot was performed at a higher operating pressure, the PCB measurements from each shot are normalized by the shot mean.

Figure 23 shows the normalized PSD of the diaphragm and piston shots. Over the entire frequency range of interest, the piston power spectra is below that of the diaphragm shot. A quantitative measure of the noise reduction was done by taking the ratio of the normalized piston PSD to the normalized diaphragm PSD over the frequency range of interest. Figure 24 shows this ratio for one test. In this case, the mean across 10 - 100 kHz was found to be 0.596, indicating a 40% noise reduction using the piston starting technique.

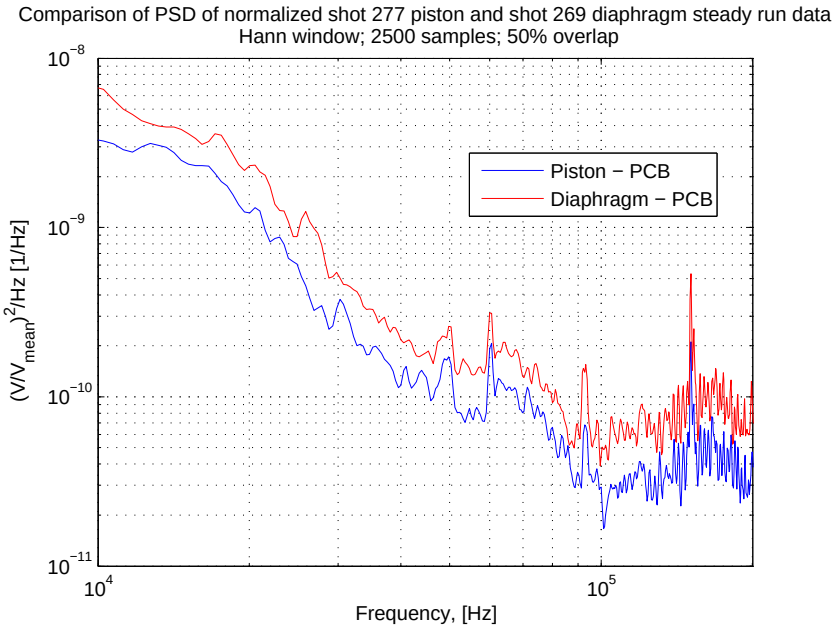

Figure 23: Comparison of piston and diaphragm PSD. Each PSD is performed on normalized data from the PCB.

5.4 Bench Test Uncertainty Analysis

Stopper location measurements during bench testing were made using a Keyence model LK-G407 high-speed, high-accuracy, CCD Laser Displacement Sensor. The position measurement sampling frequency was set at 20 kHz. The limiting uncertainty of the measurement comes from the digitization process. The digitizer has an uncertainty of 0.05% FSO (20V) corresponding to ±0.1 mm [Keyence, 2007]. The resolution uncertainty of the digitizer

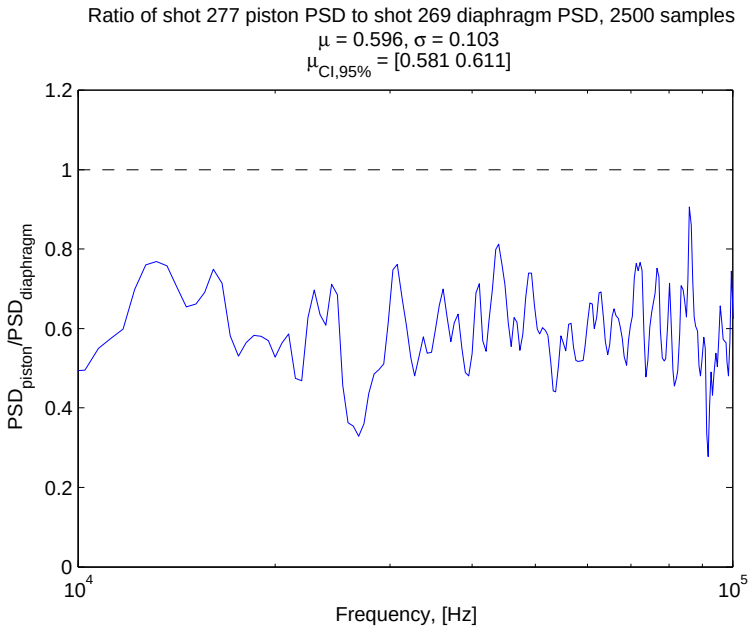

Figure 24: Ratio between the normalized piston PSD and diaphragm PSD.

is negligible compared to the standard uncertainty.

Figure 25 shows the experimental and numerical piston speeds plotted on the same graph with upper and lower bounds on the experimental data. From 17 ms to 27 ms (after the transient start time) the numerical data falls within the uncertainty range of the experimental data.

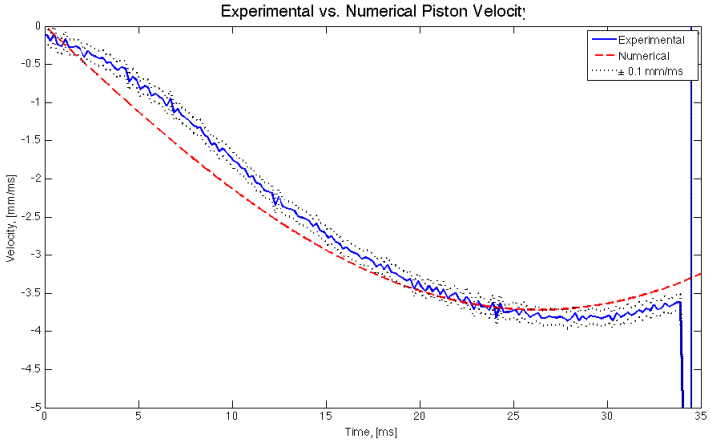

Figure 25: Comparison of the numerical and experimental bench test velocity with upper and lower bounds on the experimental velocity.

5.5 Ludwieg Tube Uncertainty Analysis

The data collected from the full-scale tests consist of just the pressure measurements using the Kulite and PCB sensors. Both of these sensors are run through a 14-bit digitizer, which introduces resolution uncertainty. The Kulite sensor has a ±0.1% FSO non-linearity, hysteresis, and repeatability combined uncertainty with an "infinitesimal" resolution. This leads to an uncertainty of the Kulite sensor of ±8.618 kPa. The PCB sensor has a resolution of 0.021 kPa and a non-linearity uncertainty of ±1.0% FSO, or ±13.79 kPa. This is significantly more than the resolution of the device, so the uncertainty in the PCB measurements is ±13.79 kPa.

The digitizer is a 14-bit system; thus, its resolution uncertainty for a ±5 V range is

$$\begin{aligned} u_{digit} &= \pm\frac{1}{2}\frac{10V}{2^{14}\text{bits}} \\ &= \pm 0.305mV \end{aligned} \tag{18}$$

When u_{digit} is converted to kPa for the Kulite transducer, this uncertainty is $u_{digit,K} = 0.1073$ kPa. This uncertainty is significantly less than the combined non-linearity, hysteresis, and repeatability uncertainty, and is thus neglected.

While the Kulite sensor is used to make actual stagnation pressure measurements, the pressure data from the PCB sensor is exclusively used for spectral analysis. As a way of measuring the uncertainty in the spectral analysis, the number of samples used in the Hann window was changed from 2500 to a lower case (1000 samples per window) and an upper case (10000 samples per window). Figure 26 shows the ratio between the piston and diaphragm (shot 269) PSD for each window size. As can be seen, the mean remains around 0.59, while the standard deviation increases at larger sampling windows. The upper and lower bounds on the 95% confidence interval also remains mostly the same for the three cases. From these results, the window size does not affect the reduction in noise conclusions.

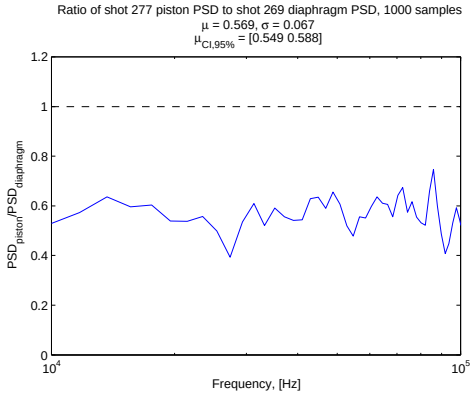

(a)

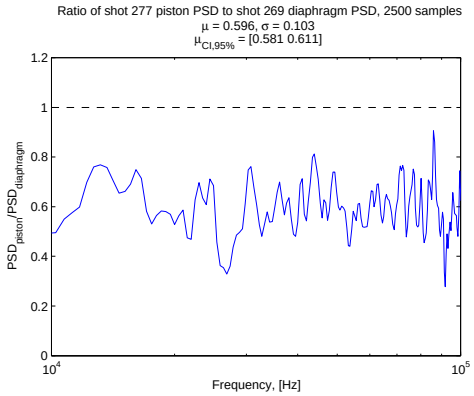

(b)

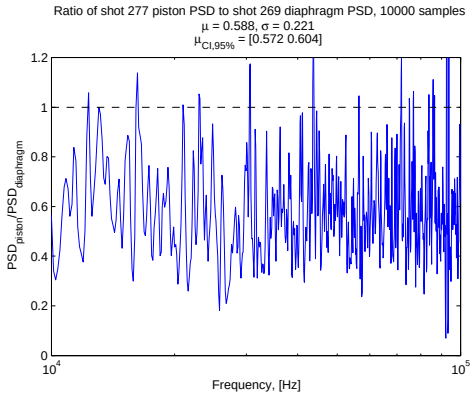

(c)

Figure 26: Ratio of piston to diaphragm PSD for window sizes of a) 1000 samples/window, b) 2500 samples/window, and c) 10000 samples/window.

6 Conclusions

In this project, a novel starting device was successfully designed, built, installed, and tested in the GALCIT Ludwieg tube. The new device met all of the initial design criteria. The stopper successfully sealed the low-pressure driven side from the high-pressure driver side prior to the run. The piston successfully started the tunnel quickly enough to maintain a sufficiently long run time. Overall operational run time was also greatly reduced, as opening the tunnel between each run to replace the burst diaphragm is no longer necessary. This also slightly reduces the amount of compressed nitrogen needed to perform each test run. Finally, from preliminary steady run pressure data, the test section freestream noise content is approximately 40% lower in the 10-100 kHz frequency range with the piston starting the tunnel. This reduction is based on the comparison of a power spectral density analysis of normalized PCB pressure data from each starting configuration. Further experimental data is necessary to confirm these results.

6.1 Future Work

Future work should focus on characterization of the tunnel operation with the piston starting configuration. Additional PCB pressure transducer data will create a more complete data set for the steady run stagnation pressure PSD analysis. Kulite pressure transducer data sampled at appropriate frequencies during the steady run time should also be recorded for the diaphragm and piston configurations. These data sets will improve stagnation pressure PSD comparisons between the starting configurations. Ideally, actual freestream static pressure fluctuation measurements in the test section will also be made for both starting configurations using focused laser doppler interferometry [Parziale, 2013].

If necessary, further noise reduction may be possible with slight redesign of the piston housing. In its current configuration, the rectangular ties (spider legs) may be shedding vortices into the nozzle throat (the ties are exposed to an effective Reynolds number of approximately 13,000. This lies in the range where vortex shedding off a rectangular bar is expected to occur). A more aerodynamic spider leg profile perpendicular to the flow may help reduce this vortex shedding. Also, reorganization of the pressure lines entering the piston will allow for easier movement of the stopper back into the nozzle after a test has been performed.

References

J. D. Anderson. *Modern compressible flow with historical perspective*. McGraw-Hill Science/Engineering/Math, 2003.

M. Estorf, T. Wolf, and R. Radespiel. Experimental and numerical investigations on the operation of the hypersonic ludwieg tube Braunschweig. *Proceedings of the Fifth European Symposium on Aerothermodynamics for Space Vehicles (ESA SP-563)*, November 2004.

Keyence. *LK-G Series User's Manual*, September 2007.

N. Parziale. *Slender-Body Hypervelocity Boundary-Layer Instability*. PhD thesis, California Institute of Technology, 2013.

Parker Pneumatic. *4MA SERIES NFPA PNEUMATIC CYLINDER*, 2014. URL http://www.parker.com/portal/site/PARKER/.

E. Reshotko. Paths to transition in wall layers. Papers presented during the AVT-151 RTO AVT/VKI Lecture Series. NATO Science and Technology Organization, 2008.

T. Vezin, S. Levine, and N. Bitter. Optical and pressure measurements of tunnel noise in the ludwieg tube. *Ae104c Report*, June 2011.

A Data

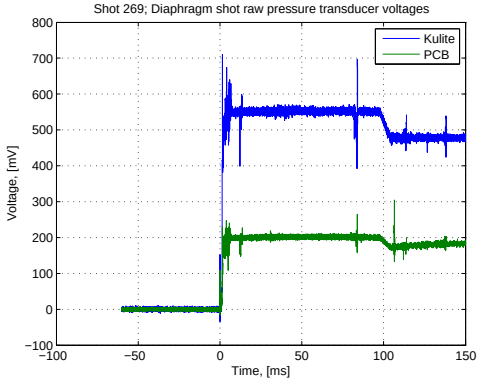

(a)

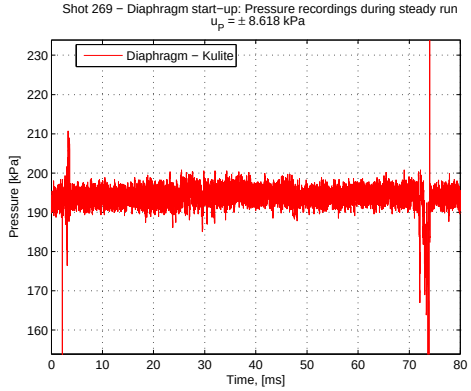

(b)

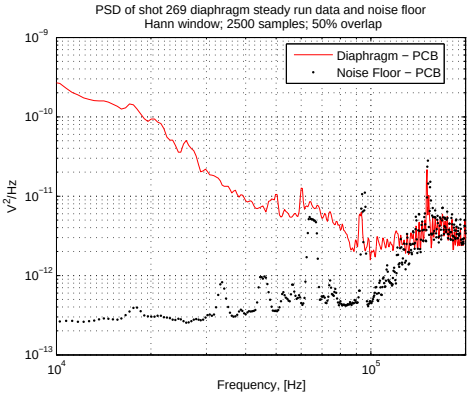

(c)

Figure 27: Diaphragm shot 269 data of a) raw voltage measurements, b) steady run Kulite pressure measurements, and c) PCB transducer PSD at 2500 samples/window.

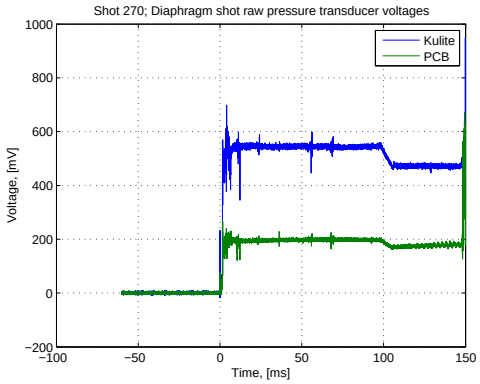

(a)

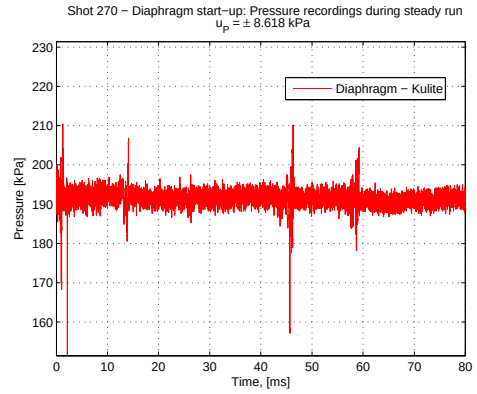

(b)

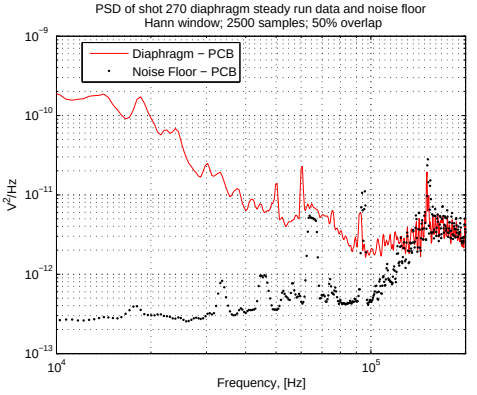

(c)

Figure 28: Diaphragm shot 270 data of a) raw voltage measurements, b) steady run Kulite pressure measurements, and c) PCB transducer PSD at 2500 samples/window.

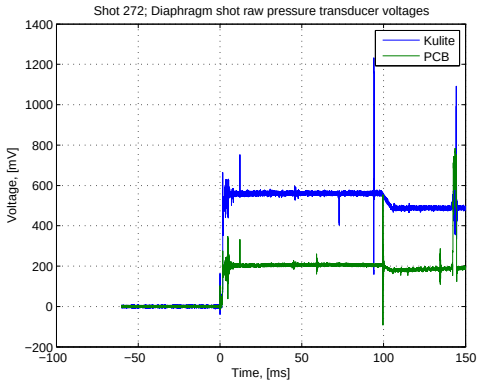

(a)

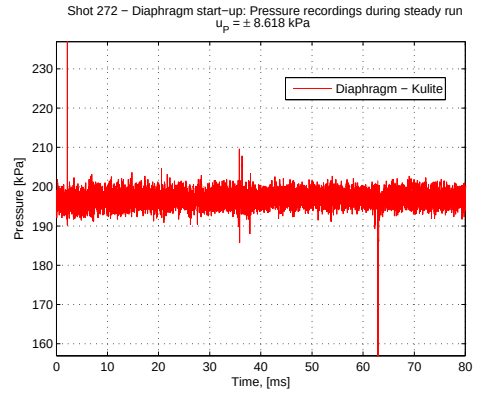

(b)

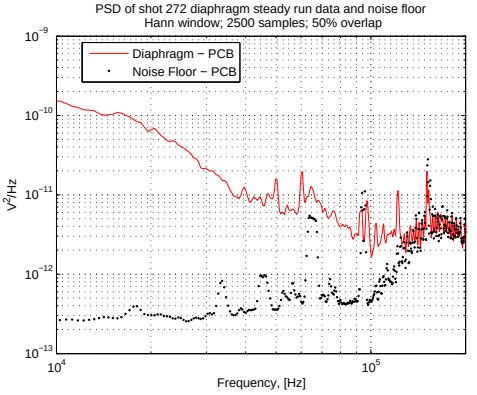

(c)

Figure 29: Diaphragm shot 272 data of a) raw voltage measurements, b) steady run Kulite pressure measurements, and c) PCB transducer PSD at 2500 samples/window.

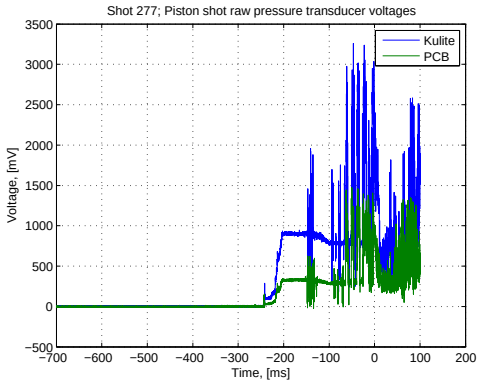

(a)

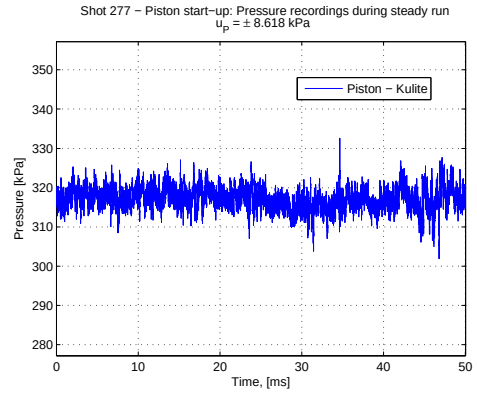

(b)

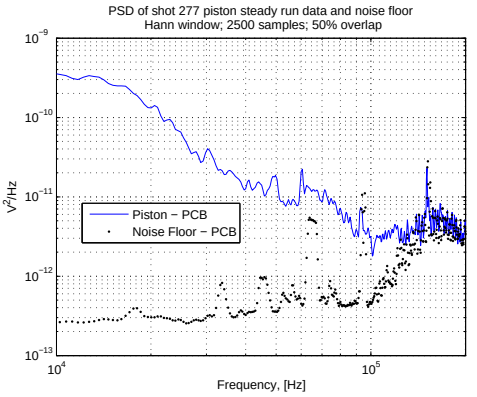

(c)

Figure 30: Piston shot 277 data of a) raw voltage measurements, b) steady run Kulite pressure measurements, and c) PCB transducer PSD at 2500 samples/window.

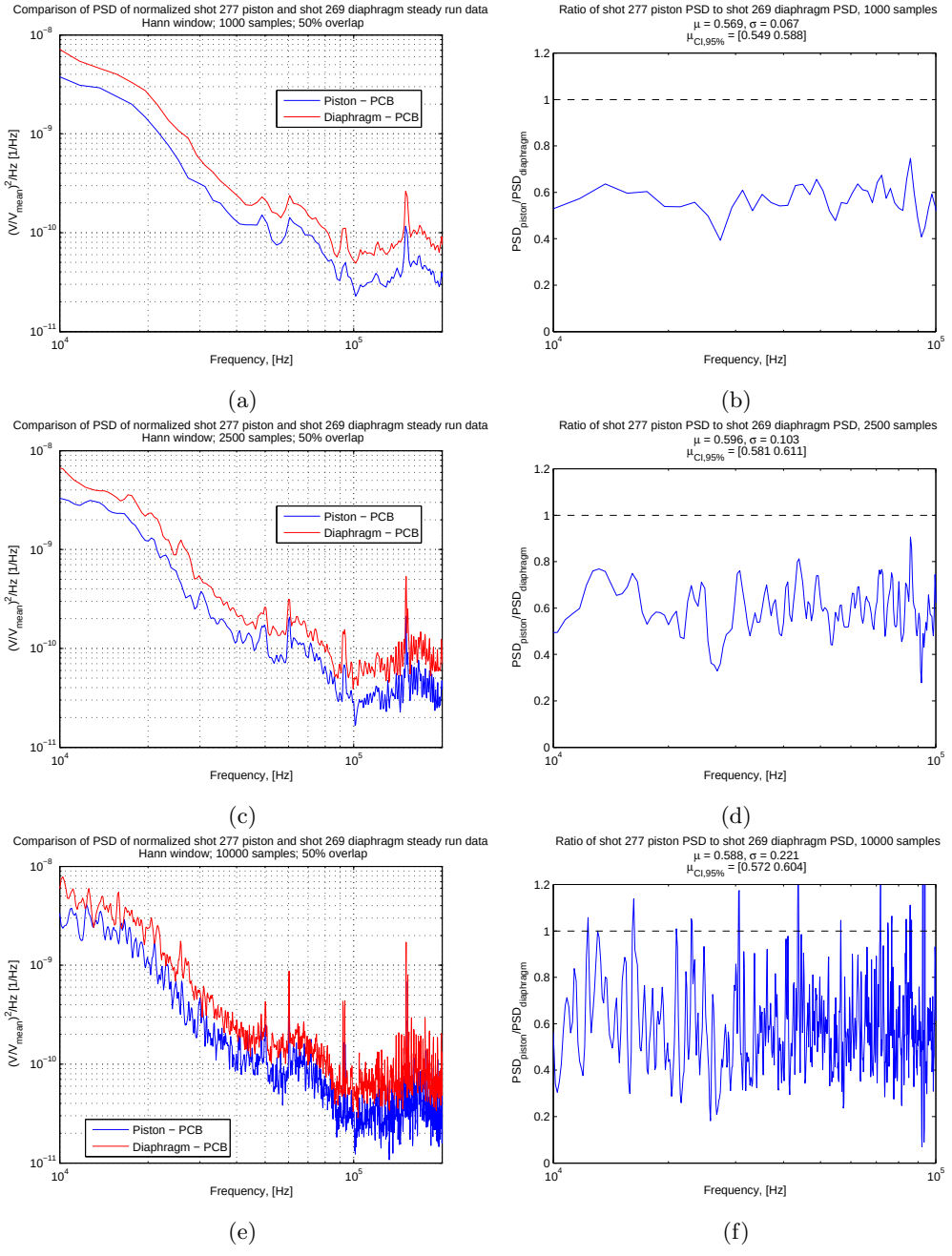

Figure 31: PSD comparisons and ratios of diaphragm shot 269 and piston shot 277 at a-b) 1000, c-d) 2500, and e-f) 10000 samples/window.

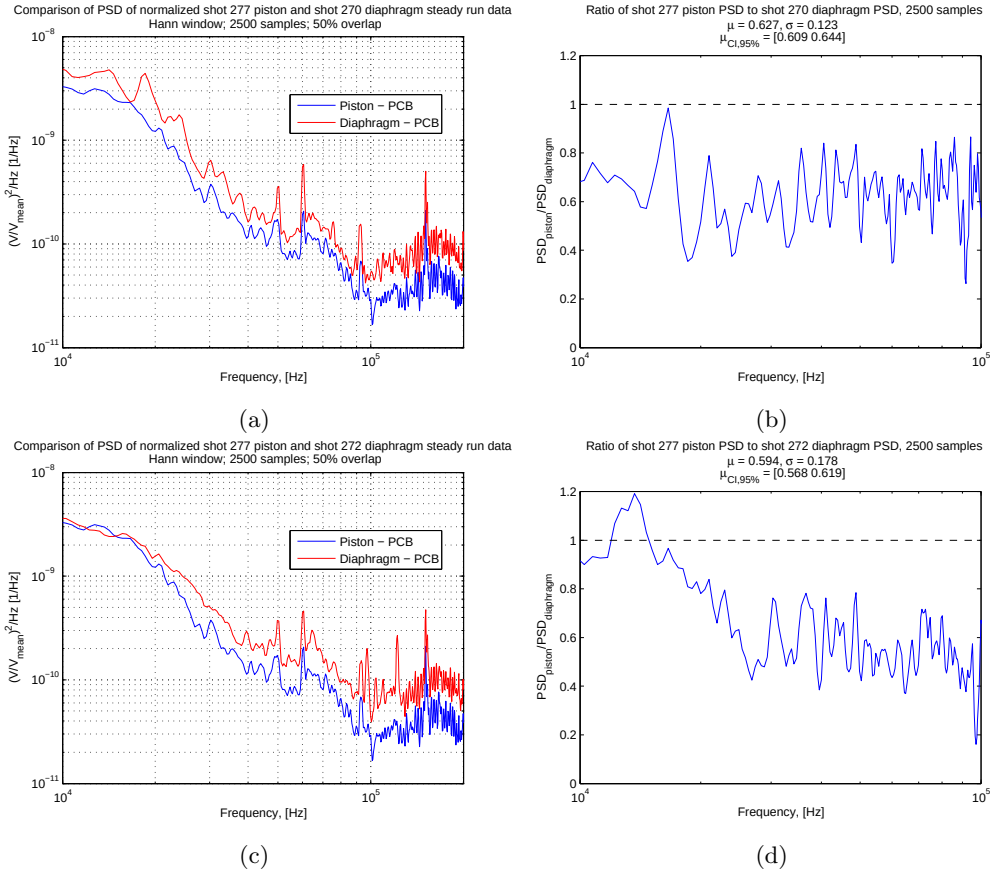

Figure 32: PSD comparison of a-b) diaphragm shot 270 and c-d) diaphragm shot 272 with piston shot 277 at 2500 samples per window.

B Facility Pictures

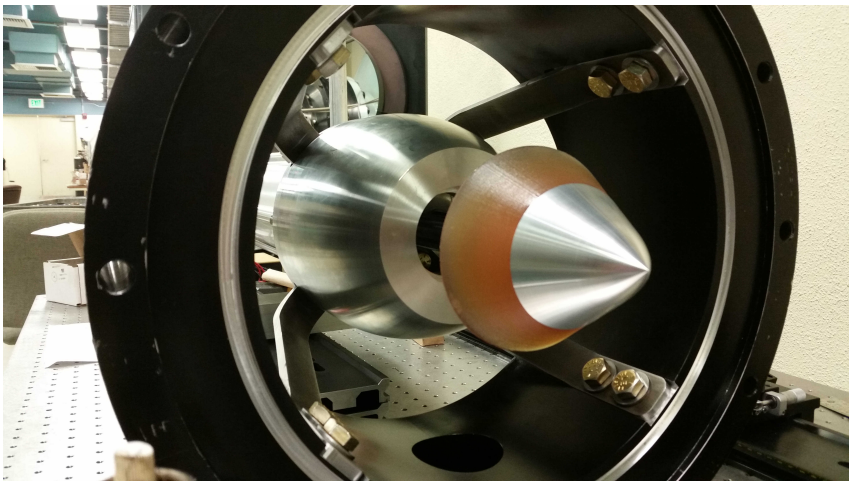

Figure 33: Front view of piston-stopper system during bench testing.

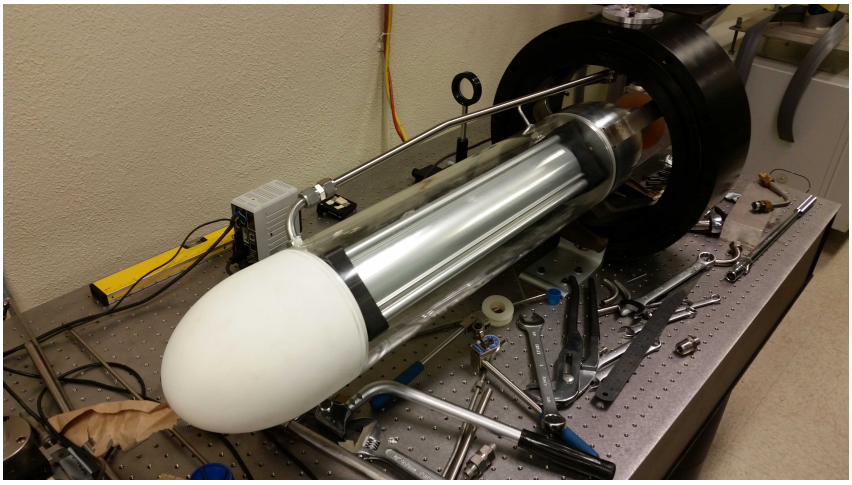

Figure 34: Rear view of fully assembled piston-stopper system outside the Ludwieg tube, including steel plumbing and acrylic housing.

Figure 35: Piston-stopper system installed in the Ludwieg tube with the front bumper and stopper removed, showing the tie support connections.

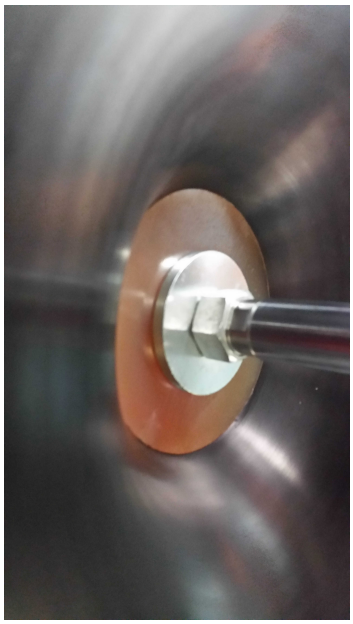

Figure 36: Stopper fully seated in the converging section of the nozzle.

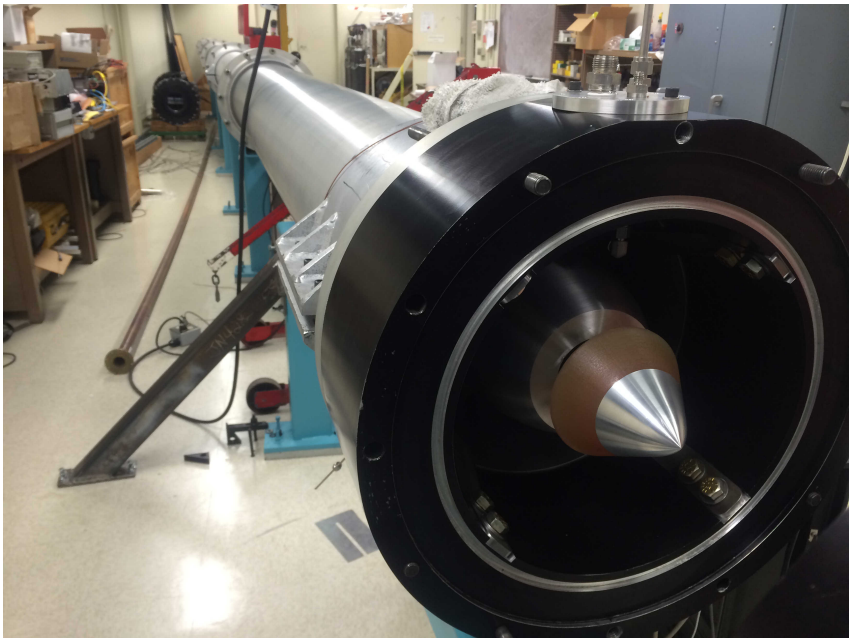

Figure 37: Fully assembled piston-stopper system in the Ludwieg tube prior to closing the tube for testing.

C Installation of Piston

First, the four support ties and the front end cap are connected with four cap screws and washers. The cap screws should be loosely secured so the ties have a small amount of free movement. A lubricant should be used as the end cap is aluminum and the cap screws are steel. Figure 38 shows this stage of the assembly.

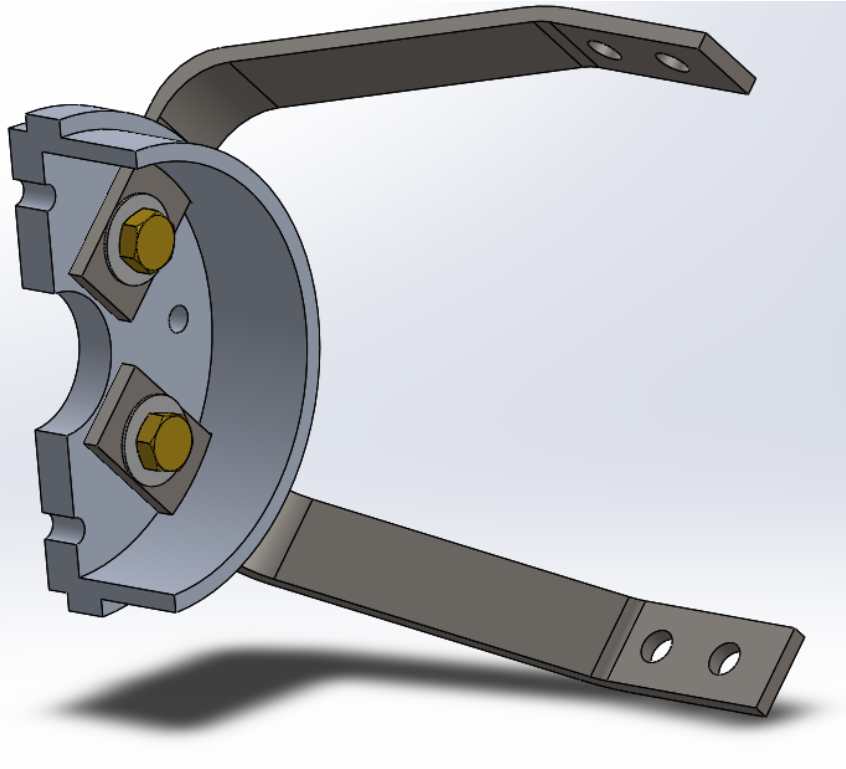

Figure 38: Section view of the end cap and ties prior to installation.

Then, with the injector flange off of the tunnel, the end cap and ties are slid from the front into the four cutouts in the injector flange. Then, eight cap screws and washers are lubricated and installed, securing the ties and front end cap to the injector flange. The cap screws should be tightened in stages to ensure the end cap remains centered. Figure 39 shows the end cap and ties attached to the injector flange.

The acrylic housing is slid over the piston, already fitted with NPTF/Swagelok fittings and the rear end cap is inserted and attached with four washers and nuts. The rear fairing is screwed onto the rear end cap, and all necessary tubing running to the piston is installed. This completed assembly is put into the Ludwieg tube driver section. Then, the injector flange and front end cap are installed on the nozzle. Figure 40 shows the assembly at this stage.

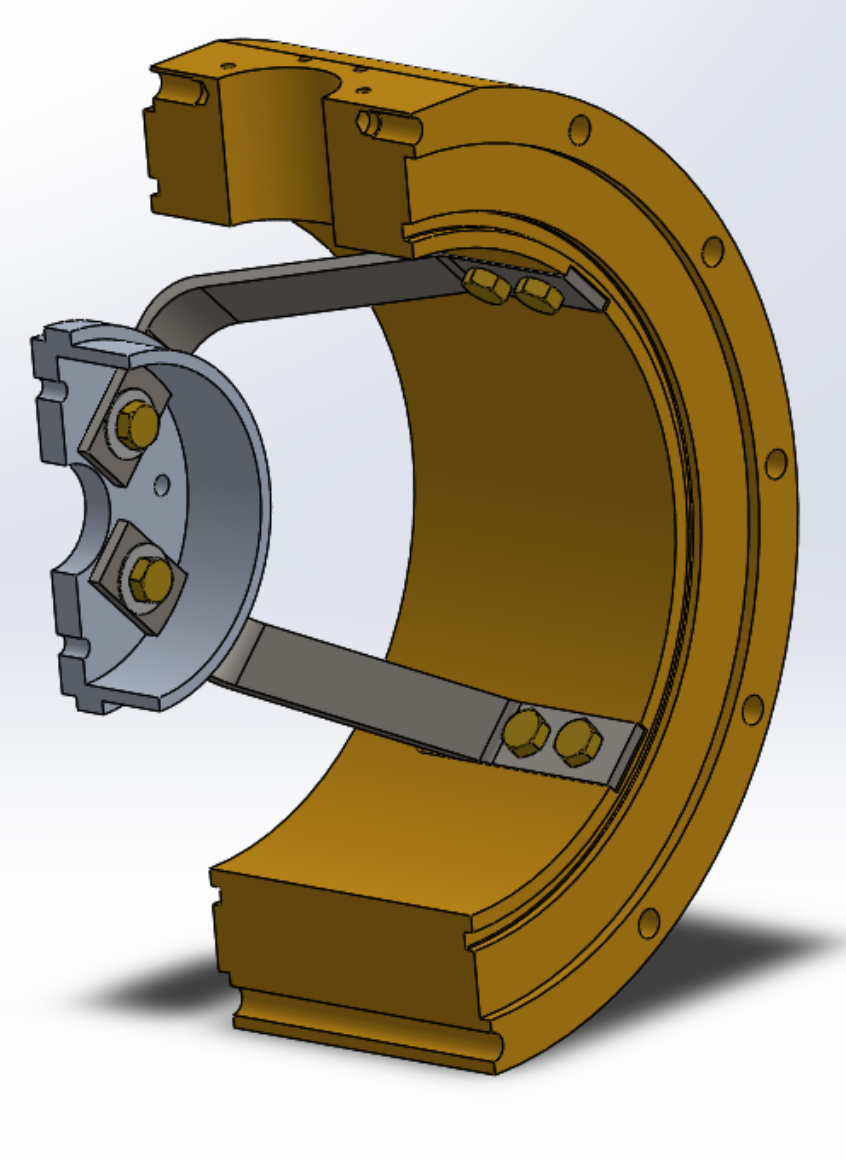

Figure 39: Section view of the end cap, ties, and injector flange prior to installation on the Ludwieg tube.

The piston assembly is lifted from the Ludwieg tube and secured to the front end cap with four washers and nuts. Figure 41 shows the piston assembly attached to the front end cap with the injector flange attached to the nozzle.

Finally, the driver tube is brought up against the injector flange and the flange is transferred from the nozzle to the driver section. Then, the two halves are separated again, the piston shaft is pulled out towards the nozzle, and the front bumper threads are lubri-

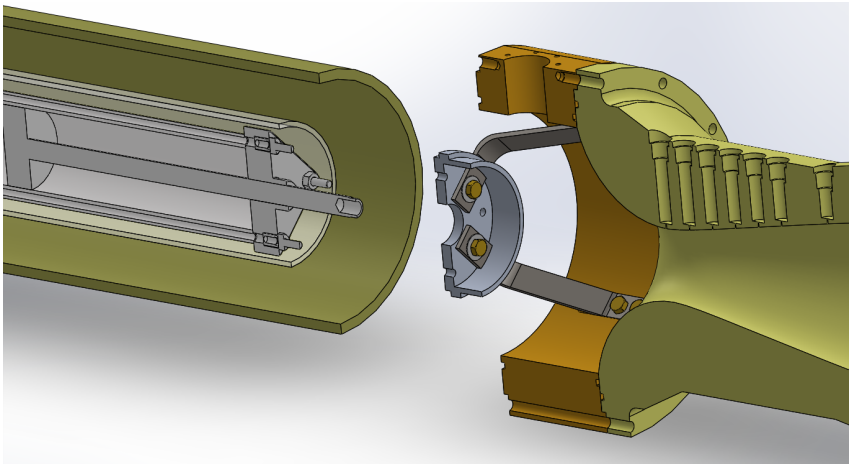

Figure 40: Section view of the end cap, ties, and injector flange installed on the nozzle with the piston assembly in the driver section.

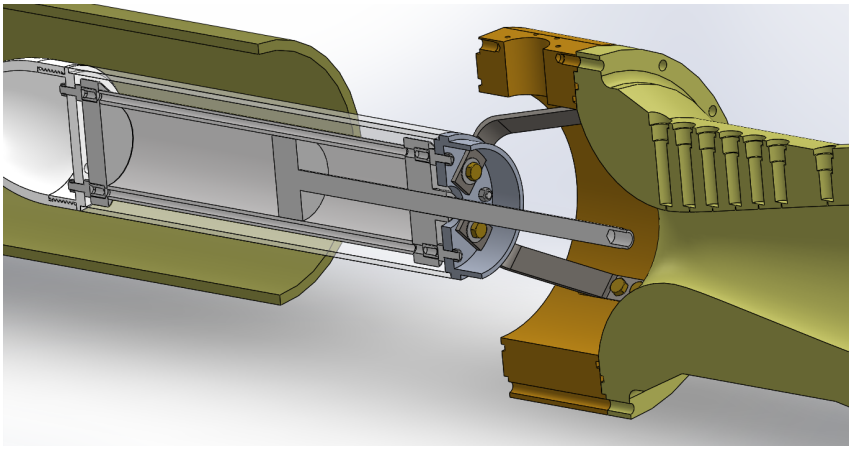

Figure 41: Section view of the piston attached to the front end cap, installed on the nozzle.

cated and threaded onto the front end cap. Finally, the stopper threads are lubricated and threaded into the piston shaft. The plumbing into the injector flange is secured and the final opened configuration is shown in Figure 42.

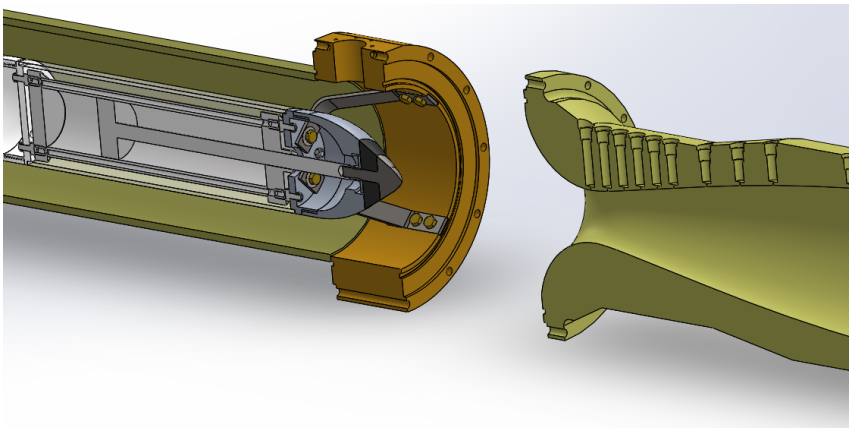

Figure 42: Section view of the piston assembly complete.

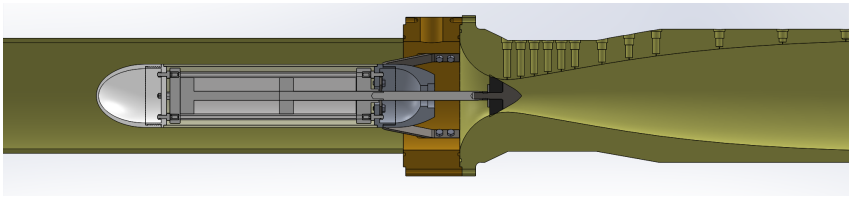

Figure 43: Section view of the assembled piston setup in the extended configuration.

D Matlab Code

In this appendix, portions of the Matlab code used to analyze the piston position are reproduced. Smaller functions that calculate isentropic flow relations and pressures or densities are omitted.

D.1 Main Piston Position Code

```
% Written by Jason Schlup and Rich Kennedy for Ae104c project  New
% starting device of the GALCIT Ludwieg tube, Spring 2014.
%
% Main function for calculating the piston position and velocity for the
% Ludweig tube. The piston is facing to the left and the cylinder is
% pressurized on the left side of the piston head to open the tunnel.
clear all
close all
clc

%% Global variables
global xl_i xr_i Cl Cr gamma m_piston A_p A_out D L_tube D_tube mr ml P_atm f

%Air properties
gamma=1.4;
P_atm=14.7; %Atmospheric pressure, lbf/in^2

% Careful of definition of Cf and f.  Inconsistencies in many sources.
% The factor of 4 should help determine which number is which.
Cf=0.02;
f=4*Cf; %Friction factor
D_tube=0.5; %Diameter of vent tube, [in]
L_tube=20; %Length of vent tube, [in]

%
% English Units
%
R = 53.3533*12; %in lbf/lbR
T = 77 + 459.67; %R

D = 4; %Piston inner diameter, [in]
cyl_length = 18; %Total length of cylinder, [in]

%NOTE: The 32.2/12 gets the units correct in the pistonode.m code. DO NOT REMOVE. To change
      the mass of the piston, just edit the first number.
m_piston = 9.27/32.2/12; %lbm/(in/s^2)
xl_i = 7; %Length of the cylinder that is pressurized, [in]

%xl_i = 8.5; %Used for experimental comparison

A_p = pi*(D/2)^2 %Piston area, [in^2]
A_out = pi*(D_tube/2)^2 %Tube vent area, [in^2]
F = 910; %Force requird to open the tunnel, [lbf]
Pi = F/A_p %Pressure on the right side of piston, [psi]

xr_i = cyl_length    xl_i ; %Total stroke length of the piston, [in]
Vr_i = A_p*xr_i %Initial volume on right side of piston, [in^3]
Pr = 14.7; %Initial stagnation pressure on right side of piston, [psi]
```

```
mr = Pr*Vr_i/(R*T) %Initial mass on right side of piston, [lbm]
Cr = Pr*Vr_i^gamma/mr^gamma; %Isentropic flow constant based on initial parameters

Vl_i = A_p*xl_i %Initial volume on left side of piston, [in^3]
Pl = Pi + Pr; %Initial pressure on left side of piston, [psi]

%Pl = 31.91; %Used with experimental data comparison 220 kPa

ml = Pl*Vl_i/(R*T); %Mass of air on the left side (constant), [lbm]
Cl = Pl*Vl_i^gamma/ml^gamma; %Isentropic flow constant based on initial parameters


%ODE45 parameters
x_init =[0 0 mr]; %Initial piston position, velocity, and mass of air on the right side of the piston
t_iter =[0:0.0001:.050]; %Time vector for ode45

[t x] = ode45('pistonode', t_iter , x_init );

% Recalculate the time varying pressures on the left and right sides of the
% piston
Pl=Cl.*ml^gamma./((xl_i+x(:,1))*A_p).^gamma;
Pr=Cr.*x(:,3).^gamma./((xr_ix(:,1) )*A_p).^gamma;
figure(1)
hold on
plot(t,x(:,1),'r','LineWidth',2)
xlabel('Time, [s]');
ylabel('Position, [in]');
title('Piston position from starting location vs time, Pr = 1 atm');
grid on


figure(2)
hold on
plot(t,x(:,2),'r','LineWidth',2)
xlabel('Time, [s]');
ylabel('Velocity, [in/s]');
title('Piston velocity vs time, Pr = 1 atm');
grid on

figure(3)
plot(t,Pl,t,Pr)
xlabel('Time, [s]');
ylabel('Pressure, [psi]');
legend('Left side','Right side','Location','NE');
title('Pressure on left and right side of piston vs time, L = 12 in, P = 1 atm');
grid on

figure(4)
hold on
plot(t,x(:,3));
xlabel('Time, [s]');
ylabel('Mass, [lbm]');
title('Mass on right side of piston vs time');
grid on
```

D.2 Piston ODE Code

```
% Written by Jason Schlup and Rich Kennedy for Ae104c project New
% starting device of the GALCIT Ludwieg tube, Spring 2014.
```

```
%
%Calculates the piston position, velocity, and right hand side mass.
function dxdt = pistonode(t,x)

global xl_i xr_i Cl Cr gamma m_piston A_p ml mr A_out

%x(1) = x(t), x(2) = v(t), x(3) = m(t) on the right hand side
dxdt = zeros(size(x));

P1_stag=Cr*(xr_ix(1)) ^( gamma)*x(3)^gamma*A_p^(gamma);
M1=getPistonOutletMach(x(1),x(3));
rho_stag=x(3)/((xr_i x(1))*A_p);

%dxdt(1) = v(t), dxdt(2) = a(t), dxdt(3) = mdot(t)
dxdt(1)=x(2);
dxdt(2)=((Cl*ml^gamma)/(xl_i+x(1))^gamma(Cr*x(3)^gamma)/(xr_ix(1))^gamma)*A_p^(1gamma)/m_piston;
dxdt(3)=sqrt(gamma*P1_stag*getPressureRatioIFR(M1)*rho_stag*getDensityRatioIFR(M1))*M1*A_out;
end
```

D.3 Piston Outlet Mach Number Code

```
% Written by Jason Schlup and Rich Kennedy for Ae104c project New
% starting device of the GALCIT Ludwieg tube, Spring 2014.
%
% Given the position of the piston and the mass of air on the right side of
% the piston, calculate the Mach number leaving the piston cylinder such
% that the stagnation pressure based on the Mach number leaving the vent
% tubing is equal to ambient pressure.

function M1 = getPistonOutletMach(x, m)

% Global variables used in this function include the specific heat ratio,
% diameter and length of the vent tubing, the initial total length right of
% the piston, the isentropic constant, piston area, ambient pressure, and
% friction factor
global gamma D_tube L_tube xr_i Cr A_p P_atm f

% Desired tolerance for iteration
TOL = 1e8;

% Calculates the stagnation pressure right of the piston given the current
% mass of air in the piston. P=Cr*(m/V)^gamma
P1_stag=Cr*((xr_ix)*A_p)^(gamma)*m^gamma;

% fL/D for the actual vent tube length and diameter
FLoD=f*L_tube/D_tube;

% Upper and lower bounds on the vent tube inlet Mach number. The lower
% bound is always very close to zero, while the upper bound is found by
% calculating the maximum inlet Mach number from the Fanno flow
% calculations
M1_upper=getMaximumMachFF(FLoD).001;
M1_lower=1e6;

% Upper and lower bounds on the outlet Mach number from Fanno flow
% calculations. For details on this, see the function "getOutletMach"
M2_upper=getOutletMach(M1_upper);
M2_lower=getOutletMach(M1_lower);

```

```
% Static pressure at the vent tube inlet from isentropic flow relations
P1_static_upper_IFR=P1_stag*getPressureRatioIFR(M1_upper);
P1_static_lower_IFR=P1_stag*getPressureRatioIFR(M1_lower);

% Static pressure at the vent tube outlet from Fanno flow pressure ratios
P2_static_upper_FF=getOutletStaticPressureFF(M1_upper,M2_upper,P1_static_upper_IFR);
P2_static_lower_FF=getOutletStaticPressureFF(M1_lower,M2_lower,P1_static_lower_IFR);

% Stagnation pressure at the vent tube outlet from isentropic flow
% relations
P2_stag_upper_IFR=P2_static_upper_FF/getPressureRatioIFR(M2_upper);
P2_stag_lower_IFR=P2_static_lower_FF/getPressureRatioIFR(M2_lower);

diff=1;
iter=1;

% Bisection method for finding the inlet Mach number
while(abs(diff)>TOL)

    % New guess of M1 is the average of the current upper and lower bounds
    % of M1
    M1_guess=(M1_upper+M1_lower)/2;

    % Calculate M2, P1, P2, and P2,t from isentropic and Fanno flow
    % relations
    M2_guess=getOutletMach(M1_guess);
    P1_static_guess_IFR=P1_stag*getPressureRatioIFR(M1_guess);
    P2_static_guess_FF=getOutletStaticPressureFF(M1_guess,M2_guess,P1_static_guess_IFR);
    P2_stag_guess_IFR=P2_static_guess_FF/getPressureRatioIFR(M2_guess);

    % Take the difference between the stagnation pressure from the guessed
    % value of M1 and atmospheric pressure
    diff=P2_stag_guess_IFRP_atm;

    % Determine new upper and lower bounds based on the sign of diff
    if diff>0
        M1_lower=M1_guess;
        M1_upper=M1_upper;
    else
        M1_lower=M1_lower;
        M1_upper=M1_guess;
    end

    iter=iter+1;

    % If no root has been found for the given tolerance after 100
    % iterations, the flow is likely choked. Thus, break from the for loop
    % and the inlet Mach number will be equal to the maximum Mach number
    % for choked flow
    if iter==100
        break
    end

end

M1=M1_guess
iter

end
```

D.4 Data Analysis Code

```
%%%KULITE CALIBRATION  19.600 mV/PSI A

clear all
close all
clc

%%% Piston data
data1=importdata('C:\Users\Jason_Schlup\Dropbox\Caltech\Classes\Ae_104c\Piston_
    Shots\shot_277\shot_277_Ludwieg_Tube_data.mat');
shot1 = '277';
start_method_1 = 'Piston';

start_time_1=data1(1,1);
Fs=2e6;

%%% Plot all piston raw data %%%
f=figure();
plot(data1(:,1)*1000,data1(:,2)*1000,data1(:,1)*1000,data1(:,3)*1000);
xlabel('Time, [ms]');
ylabel('Voltage, [mV]');
legend('Kulite','PCB');
 title (['Shot ',shot1,'; ',start_method_1,' shot raw pressure transducer voltages']);
grid on;

filename=sprintf('shot%s_raw',shot1);

set(f,'Units','Inches');
pos = get(f,'Position');
set(f,'PaperPositionMode','Auto','PaperUnits','Inches','PaperSize',[pos(3), pos(4)])
saveas(f,filename,'fig')
print(f,filename,' dpdf',' r300')

begin_shot_time_1 = 0.20;
end_shot_time_1 = 0.15;
begin_index_1=(begin_shot_time_1start_time_1)*Fs;
begin_index_1=int64(begin_index_1);



%%% Diaphragm data
data2=importdata('C:\Users\Jason_Schlup\Dropbox\Caltech\Classes\Ae_104c\Diaphragm_
    Test\shot_272\shot_272_Ludwieg_Tube_data.mat');
shot2 = '272';
start_method_2 = 'Diaphragm';

start_time_2=data2(1,1);

%%% Plot all diaphragm raw data %%%
f=figure();
plot(data2(:,1)*1000,data2(:,2)*1000,data2(:,1)*1000,data2(:,3)*1000);
xlabel('Time, [ms]');
ylabel('Voltage, [mV]');
legend('Kulite','PCB');
 title (['Shot ',shot2,'; ',start_method_2,' shot raw pressure transducer voltages']);
grid on;

filename=sprintf('shot%s_raw',shot2);
set(f,'Units','Inches');
```

```
57  pos = get(f,'Position');
58  set(f,'PaperPositionMode','Auto','PaperUnits','Inches','PaperSize',[pos(3), pos(4)])
59  saveas(f,filename,'fig')
60  print(f,filename,'dpdf','r300')
61
62
63  begin_shot_time_2 = 0.01;
64  end_shot_time_2 = 0.09;
65  begin_index_2=(begin_shot_time_2start_time_2)*Fs;
66  begin_index_2=int64(begin_index_2);
67
68  %%% Noise floor data
69
70  noise_data=importdata('C:\Users\Jason Schlup\Dropbox\Caltech\Classes\Ae 104c\Noise
        Floor\shot_278\shot_278_Ludwieg_Tube_data.mat');
71  shot3 = '278';
72  start_method_3 = 'N/A';
73
74
75  %%% Extract steady run data for piston
76  time1=data1(begin_index_1:begin_index_1+(end_shot_time_1begin_shot_time_1)*Fs,1);
77  voltage1_1=data1(begin_index_1:begin_index_1+(end_shot_time_1begin_shot_time_1)*Fs,2);
78  voltage2_1=data1(begin_index_1:begin_index_1+(end_shot_time_1begin_shot_time_1)*Fs,3);
79
80  uncert_p='8.618';
81
82  %%% Extract steady run data for diaphragm
83  time2=data2(begin_index_2:begin_index_2+(end_shot_time_2begin_shot_time_2)*Fs,1);
84  voltage1_2=data2(begin_index_2:begin_index_2+(end_shot_time_2begin_shot_time_2)*Fs,2);
85  voltage2_2=data2(begin_index_2:begin_index_2+(end_shot_time_2begin_shot_time_2)*Fs,3);
86
87  %%% Plot pressure measurements for piston
88  f=figure();
89  plot((time1 min(time1))*1000,voltage1_1*1000/19.6*6.895,'b') ;
90  xlabel('Time, [ms]');
91  ylabel('Pressure [kPa]');
92  xlim([(min(time1)min(time1))*1000,(max(time1)min(time1))*1000]);
93  ylim([mean(voltage1_1)*1000/19.6*6.89540,mean(voltage1_1)*1000/19.6*6.895+40])
94  legend('Piston  Kulite','Location','Best');
95   titlestr =sprintf('Shot %s  %s start up: Pressure recordings during steady run\n u {P} = \\pm %s
        kPa', shot1, start_method_1, uncert_p);
96   title ( titlestr );
97  grid on;
98
99  filename=sprintf('shot%s_steady',shot1);
100 set(f,'Units','Inches');
101 pos = get(f,'Position');
102 set(f,'PaperPositionMode','Auto','PaperUnits','Inches','PaperSize',[pos(3), pos(4)])
103 saveas(f,filename,'fig')
104 print(f,filename,'dpdf','r300')
105
106 %%% Plot pressure measurements for diaphragm
107 f=figure();
108 plot((time2 min(time2))*1000,voltage1_2*1000/19.6*6.895,'r');
109 xlabel('Time, [ms]');
110 ylabel('Pressure [kPa]');
111 xlim([(min(time2)min(time2))*1000,(max(time2)min(time2))*1000]);
112 ylim([mean(voltage1_2)*1000/19.6*6.89540,mean(voltage1_2)*1000/19.6*6.895+40])
113 legend('Diaphragm  Kulite','Location','Best');
```

```
114  titlestr =sprintf('Shot %s  %s start up: Pressure recordings during steady run\n u {P} = \\pm %s
         kPa', shot2, start_method_2, uncert_p);
115  title ( titlestr );
116  grid on;
117
118  filename=sprintf('shot%s_steady',shot2);
119  set(f,'Units','Inches');
120  pos = get(f,'Position');
121  set(f,'PaperPositionMode','Auto','PaperUnits','Inches','PaperSize',[pos(3), pos(4)])
122  saveas(f,filename,'fig')
123  print(f,filename,'dpdf','r300')
124
125  %%% Power spectral density of PCB
126
127  nsamp='2500';
128
129  h=spectrum.welch('hann',str2num(nsamp),50);
130  Vpsd2_1=psd(h,voltage2_1,'Fs',Fs);
131  Vpsd2_2=psd(h,voltage2_2,'Fs',Fs);
132  Vpsd_noise=psd(h,noise_data(:,3),'Fs',Fs);
133
134  %%% LogLog plot of noise floor
135  f=figure();
136  loglog(Vpsd_noise.Frequencies,Vpsd_noise.Data,'k.');
137  xlim([1e4 2e5])
138  xlabel('Frequency, [Hz]');
139  ylabel('V^2/Hz');
140  legend('Noise Floor  PCB','Location','Best');
141  titlestr =sprintf('PSD of noise floor\n Hann window; %s samples; 50%% overlap', shot1, nsamp);
142  title ( titlestr );
143  grid on;
144
145  filename=sprintf(' noise_floor_ %s',nsamp);
146  set(f,'Units','Inches');
147  pos = get(f,'Position');
148  set(f,'PaperPositionMode','Auto','PaperUnits','Inches','PaperSize',[pos(3), pos(4)])
149  saveas(f,filename,'fig')
150  print(f,filename,'dpdf','r300')
151
152
153  %%% LogLog plot of PSD for piston and noise floor
154  f=figure();
155  loglog(Vpsd2_1.Frequencies,Vpsd2_1.Data,'b',Vpsd_noise.Frequencies,Vpsd_noise.Data,'k.');
156  xlim([1e4 2e5])
157  xlabel('Frequency, [Hz]');
158  ylabel('V^2/Hz');
159  legend('Piston  PCB','Noise Floor  PCB','Location','Best');
160  titlestr =sprintf('PSD of shot %s piston steady run data and noise floor\n Hann window; %s
         samples; 50%% overlap', shot1, nsamp);
161  title ( titlestr );
162  grid on;
163
164  filename=sprintf('shot%s_psd_%s',shot1,nsamp);
165  set(f,'Units','Inches');
166  pos = get(f,'Position');
167  set(f,'PaperPositionMode','Auto','PaperUnits','Inches','PaperSize',[pos(3), pos(4)])
168  saveas(f,filename,'fig')
169  print(f,filename,'dpdf','r300')
170
171
```

```
%%% LogLog plot of PSD for diaphragm and noise floor
f=figure();
loglog(Vpsd2_2.Frequencies,Vpsd2_2.Data,'r',Vpsd_noise.Frequencies,Vpsd_noise.Data,'k.');
xlim([1e4 2e5])
xlabel('Frequency, [Hz]');
ylabel('V^2/Hz');
legend('Diaphragm  PCB','Noise_Floor  PCB','Location','Best');
 titlestr =sprintf('PSD_of_shot_%s_diaphragm_steady_run_data_and_noise_floor\n_Hann_window; %s_
      samples; 50%%_overlap', shot2, nsamp);
 title ( titlestr );
grid on;

filename=sprintf('shot%s_psd_%s',shot2,nsamp);
set(f,'Units','Inches');
pos = get(f,'Position');
set(f,'PaperPositionMode','Auto','PaperUnits','Inches','PaperSize',[pos(3), pos(4)])
saveas(f,filename,'fig')
print(f,filename,'dpdf','r300')


%Normalize voltages
voltage1_1=voltage1_1/mean(voltage1_1);
voltage2_1=voltage2_1/mean(voltage2_1);

voltage1_2=voltage1_2/mean(voltage1_2);
voltage2_2=voltage2_2/mean(voltage2_2);

Vpsd2_1=psd(h,voltage2_1,'Fs',Fs);
Vpsd2_2=psd(h,voltage2_2,'Fs',Fs);

%%% LogLog plot of PSD for piston and diaphragm
f=figure();
loglog(Vpsd2_1.Frequencies,Vpsd2_1.Data,'b',Vpsd2_2.Frequencies,Vpsd2_2.Data,'r');
xlim([1e4 2e5])
xlabel('Frequency, [Hz]');
ylabel('(V/V_{mean})^2/Hz [1/Hz]');
legend('Piston  PCB','Diaphragm  PCB','Location','Best');
 titlestr =sprintf('Comparison_of_PSD_of_normalized_shot_%s_piston_and_shot_%s_diaphragm_steady_
      run_data\n_Hann_window; %s_samples; 50%%_overlap', shot1, shot2, nsamp);
 title ( titlestr );
grid on;

filename=sprintf('shot%s_shot%s_comparison_%s',shot2,shot1,nsamp);
set(f,'Units','Inches');
pos = get(f,'Position');
set(f,'PaperPositionMode','Auto','PaperUnits','Inches','PaperSize',[pos(3), pos(4)])
saveas(f,filename,'fig')
print(f,filename,'dpdf','r300')

%%% Ratio of PCB data of piston/diaphragm
Fcutoff_upper=1e5;
Fcutoff_lower=1e4;

[~, icutoff_up]=min(abs(Fcutoff_upperVpsd2_1.Frequencies));
[~, icutoff_low]=min(abs(Fcutoff_lowerVpsd2_1.Frequencies));

ratio=Vpsd2_1.Data./Vpsd2_2.Data;
[muhat, sigmahat, muci, sigmaci] = normfit(ratio(icutoff_low:icutoff_up));

f=figure();
```

```
230  semilogx(Vpsd2_1.Frequencies,ratio,[1  1e6],[1   1], 'k   ')
231  xlim([1e4  1e5]);
232  ylim([0   1.2])
233  xlabel('Frequency, [Hz]');
234  ylabel('PSD_{piston}/PSD_{diaphragm}');
235   titlestr =sprintf('Ratio of shot %s piston PSD to shot %s diaphragm PSD, %s samples\n \\mu =
         %5.3f, \\sigma = %5.3f\n \\mu_{CI,95%%} = [%5.3f %5.3f]', shot1, shot2, nsamp, muhat,
         sigmahat, muci(1), muci(2));
236   title ( titlestr )
237
238  filename=sprintf('shot%s_shot%s_ratio_%s',shot2,shot1,nsamp);
239  set(f,'Units','Inches');
240  pos = get(f,'Position');
241  set(f,'PaperPositionMode','Auto','PaperUnits','Inches','PaperSize',[pos(3), pos(4)])
242  saveas(f,filename,'fig')
243  print(f,filename,'-dpdf','-r300')
```